

Carbon-based Materials for Li-ion Battery

Binson Babu^{*[a]}



Carbon-based materials have played a pivotal role in enhancing the electrochemical performance of Li-ion batteries (LIBs). This review summarizes the significant developments in the application of carbon-based materials for enhancing LIBs. It highlights the latest innovations in different types of carbon materials such as graphite, soft carbon, hard carbon, and various carbon nanostructures, including design and synthesis. Additionally, the feasibility of developing flexible self-supported electrodes for wearable devices is underlined. More emphasis is given to elucidating the Li-ion storage mechanisms inherent in various carbon materials, illustrating the variations in Li-storage that

arise as the structure transitions from order to disorder and from bulk to the nano realm. Furthermore, the use of carbon composites, which incorporate different alloy/conversion/intercalation type materials with carbon matrices, is discussed in view of their improved electrochemical performances in terms of energy density, power density, and cycling stability. The review underscores the growing importance of carbon materials in addressing the ever-increasing demand for high-performance energy storage solutions and also addresses the remaining challenges and future perspectives, aiming to provide future research directions.

1. Introduction

Rechargeable Li-ion batteries (LIBs) play a crucial role in developing sustainable energy storage devices, which is essential to meet the criteria to achieve clean energy transition.^[1] The application of LIBs ranges from portable electronic gadgets to large-scale sectors and takes over the whole energy storage sector due to their superior energy density over other rechargeable battery technologies. The masterminds behind the development of Li-ion batteries, John Goodenough, Stanley Whittingham, and Akira Yoshino, grabbed the Nobel Prize for chemistry in 2019. The choice of lithium metal over other elements for high-energy-density batteries lies on its high inherent specific capacity (3860 mAh g⁻¹), very low reduction potential (-3.045 V vs. standard hydrogen electrode), and a small gravimetric density of 0.534 g cm⁻³.^[2] However, the direct usage of Li-metal in rechargeable batteries, as seen in Li-metal batteries, is facing commercial challenges due to the dendrite formation over prolonged cycling. The dendrite (lithium metal crystals) formed on the surface of lithium metal during repeated lithium plating and stripping pierced through the separator and caused an internal short circuit, resulting in catastrophic failure of the battery. Replacing Li-metal electrodes with Li-ion insertion/extraction materials led to the inception of LIBs, which are now the standard for electronic devices, wireless communications, and electric vehicles, and even in large-scale power grids.^[3-5]

A LIB consists of an assembly of electrochemical cells configured in series to boost voltage or in parallel to increase capacity. Each electrochemical cell comprises both a negative (anode) and a positive (cathode) electrode (as illustrated in Figure 1a). The organic electrolytes facilitate the Li-ion shuttling between the two electrodes, separated by an ion-permeable membrane composed of materials such as glassy microfiber, microporous polymer, or cellulose, which are insulators towards the electrons. The exceptional characteristics of LIBs, including high energy density, power density, and cycle life, are reliant on the electrochemical synchronization of these components.

When charging, Li-ions migrate from the positive electrode (cathode) to the negative electrode (anode) and conversely during discharge. This shuttling of Li-ions between the electrodes has led to the nickname "Rocking chair batteries". Further, the charge storage within the battery is achieved through faradaic reactions involving redox processes that occur at the interfaces of the electrode and electrolyte. The key redox processes responsible for energy storage are intercalation, conversion, and alloy formation, and their occurrence is dictated by the choice of electrode materials. The anode materials in LIBs play a crucial part in determining the overall electrochemical performance, encompassing energy density and cycling stability. Consequently, significant efforts have been dedicated to developing highly efficient anode materials.^[6]

In the search for anode materials, carbon-based materials seem to be more beneficial and have been commercially viable in the past couple of decades. Compared to other anode materials such as metal oxides, chalcogenides, polymers, etc., carbon-based electrode materials have high thermodynamic and electrochemical stability and are highly abundant and cost-effective.^[7-11] Scheme 1 illustrates the significant advancements in carbon-based anode materials in LIBs. The first commercialized secondary LIBs introduced by Sony in 1991 used layered electrode materials such as soft carbon (petroleum coke) and LiCoO₂ as the anode and cathode, respectively, and the faradaic reaction here is due to the intercalation of Li-ions.^[12-14] This first-generation LIB shows a high voltage of about 4 V by employing propylene carbonate as solvent electrolyte and exhibits a specific energy of 80 Wh kg⁻¹ (200 Wh L⁻¹), which outperforms all the other secondary battery technology available at that time. Later, Sony replaced soft carbon with hard carbon in the second-generation LIB, achieving a higher specific energy density of 120 Wh kg⁻¹ (295 Wh L⁻¹) with an upper cut-off voltage of about 4.2 V. In the third generation LIB, Sony introduces graphite that has the advantage of flatter potential close to zero. This characteristic contributes to a remarkably high cell potential, promoting an energy density of 160 Wh kg⁻¹, which is double the energy density of nickel-metal hydride batteries.^[12,15] The Li-ions are inserted into the carbon host matrices at very low reduction potential according to the equation



[a] Dr. B. Babu

Department of Physics, School of Natural Sciences, Shiv Nadar Institution of Eminence,
NH-91, Greater Noida, Uttar Pradesh, 201314, India
E-mail: binson.babu@snu.edu.in

The carbonaceous material possesses a high theoretical capacity of 372 mAh g^{-1} for $x = 1$ and $n = 6$, and the host sites for lithium accommodation are highly dependent on various factors such as crystallinity, surface morphology, active surface area (Brunauer–Emmett–Teller, BET) and pore size distributions.^[8,16] Moreover, the state-of-the-art organic electrolytes used in LIBs have maximum oxidation potentials around 4.7 V vs. Li⁺/Li and reduction potentials close to 1.0 V vs. Li⁺/Li, which is the energy of the highest occupied molecular orbital (HOMO) and the lowest unoccupied molecular orbital (LUMO) of the electrolyte, respectively (Figure 1b). Since the insertion potential of Li-ions in carbonaceous materials is below the reduction potential of the state-of-the-art organic electrolytes with respect to the Li/Li⁺, a passive solid electrolyte interface (SEI) layer will be formed at the electrode/electrolyte interface with the expense of electrolyte during the charging of LIB. The formed SEI layer blocks the flow of electrons from the anode to the LUMO of the electrolyte and hence acquires kinetic stability. Therefore, a stable, uniform SEI layer formation is essential to avoid continuous electrolyte reduction and, hence, to ensure the long-term stability of the devices. Apart from the electrolyte compositions, electrolyte additives, etc., the physical, structural, and morphological nature of the anode materials affects the porosity, homogeneity, and strength of the SEI layer.^[17–19] For instance, the large volume change in electrode materials during Li-ion insertion or de-insertion results in the cracking of the SEI layer, which induces more electrolyte consumption over cycling and eventually leads to cell failure.^[20,21] Thus, the selection of anode materials influences the overall electrochemical performance of LIBs in terms of higher energy density and cycling stability.

Since carbonaceous materials are a viable anode choice for LIBs, a detailed investigation of structural, morphological, and chemical aspects is imperative. The application status of carbon varies depending on different forms and compatibility, ranging from active storage materials to conductive additives and other structural components. For example, graphite foam proves suitable for Li-ion storage, while carbon black (acetylene black) functions as a conductive additive in both anode and cathode

materials.^[22–24] On the other hand, the nanostructure foams of carbons, including graphene, carbon nanotubes, etc., can be utilized as active storage materials, conductive additives, and structural components incorporating with other active materials as composites due to their structural robustness and highly tunable electrical conductivity. Furthermore, highly disordered carbon materials, encompassing hard carbon, highly porous activated carbon, and biomass carbons, fall within the realm of active Li-storage materials, exhibiting significant storage capacity.^[25–28] This review focuses on the various research progress that happens in different types of carbon-based materials from the bulk to the nano realm and their influences as anode materials in the advancement of LIB technology. More detailed analyses of the Li-storage mechanisms and their variations when the structure changes from order to disorder and from bulk to the nano, influence of different electrolytes, etc., are reviewed with general conclusions and perspectives.

2. Carbon-based anode materials for LIB

Carbonaceous materials are widely accepted as promising practical anode materials for LIBs due to their electrochemical and thermal stability, low working potential, higher storage capacity, and low cost. The carbonaceous materials that are capable of reversible lithium intercalation can be generally classified as graphitic (ordered) and non-graphitic (disordered).^[30] These are all sp²-hybridized carbon atoms, which are arranged in hexagonal honeycomb covalent lattices in a 2D layer structure (graphene layer), and the layers are stacked together by means of Van der Waals forces. Graphitic carbon possesses an ordered layer structure with perfect stacking of graphene layers, e.g., graphite, whereas non-graphitic carbon does not have a long crystallographic order in the c-direction. Non-graphitic carbon has two types: graphitizable carbon/soft carbon (SC) and non-graphitizable carbon/hard carbon (HC). The formation of the different material structures strongly depends on the precursors and the heating treatment conditions during synthesis. The ordering of layers is prohibited by the strong cross-linkings of the precursors, which create nanovoids in the structures due to the gas evolution while heating. On the other hand, the state of fusion during the carbonization of the precursors evolves to soft carbon, which is highly favorable for graphitization at elevated temperatures. The level of disorder increases from soft carbon to hard carbon, whereas graphitized carbon has more structural ordering (Figure 1c). The structural disorder and reduced stacking of graphite crystals in HC and SC are clearly visible from the disappearance of the 2D band at $\approx 2685 \text{ cm}^{-1}$ in the Raman spectra as compared to the graphite (Figure 1d (i)). Besides, the sharp rise of the D band represents the turbostratic disorder and defects in HC and SC, and the degree of the disorder can be evaluated from the ratio of the D band and G band intensities. Further, the structural characterization of materials can be evaluated from the XRD spectra, where broader peaks correspond to the smaller average crystal sizes in SC and HC compared to graphite (Figure 1d (ii)). Also, the (002) peak shift towards a lower degree



Binson Babu is an assistant professor at the Department of Physics, School of Natural Science at the Shiv Nadar Institution of Eminence, Delhi-NCR, India. He received his Ph.D. in physics from the Indian Institute of Science Education and Research-Thiruvananthapuram, India in 2019. After that, he pursued his postdoctoral research at Friedrich-Schiller-University, Jena (2019–2022), and at Université catholique de Louvain, Belgium (2022–2023). He cracked the prestigious HORIZON-TMAMSCA-PF-EF fellowship in the year 2023 and received the SRG from SERB, India. His research interests focus on developing innovative electrode and electrolyte materials for the application of rechargeable batteries, supercapacitors, and hybrid-ion capacitors.

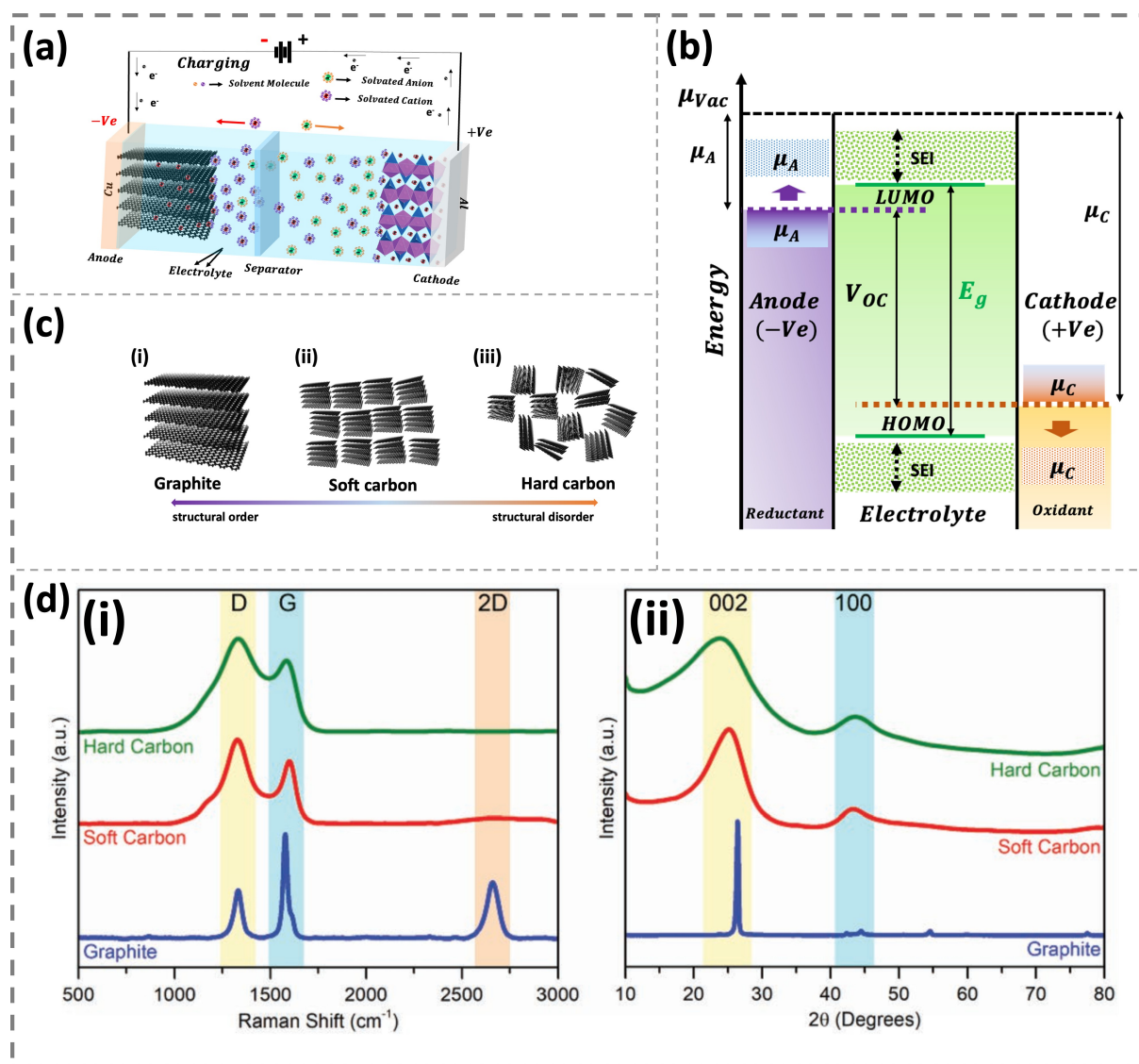
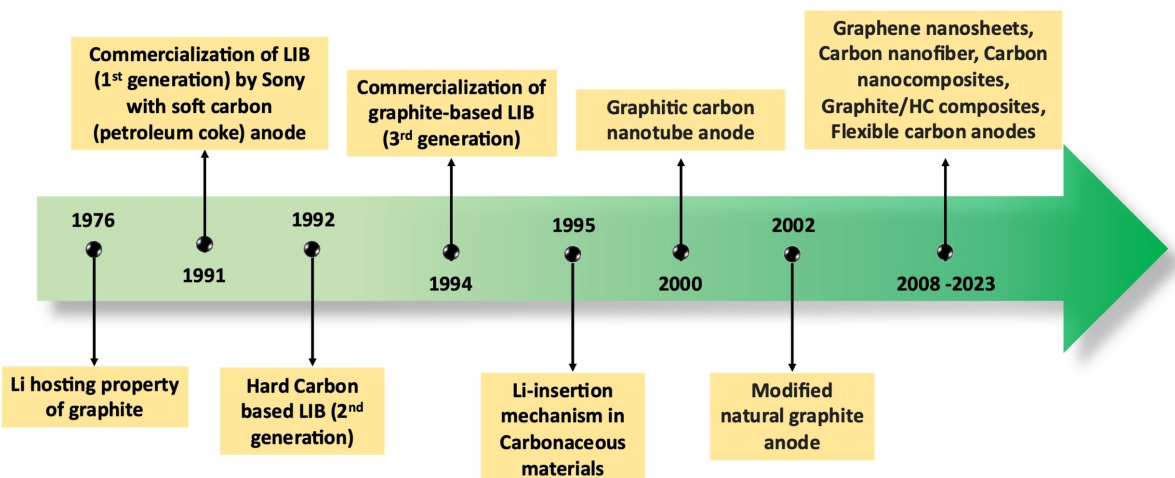


Figure 1. Schematic representation of (a) the first commercialized LIB and (b) the energy diagram of anode and cathode with relative energies of the voltage window (E_g) of a thermodynamically stable LIB. (c) Schematic illustration of the structure of (i) graphite, (ii) soft carbon, and (ii) hard carbon, and (d) their corresponding (i) Raman and (ii) XRD spectra. Reproduced from ref.^[29] Copyright 2019, with permission from Wiley-VCH.



Scheme 1. Timeline showing the significant advancements in carbon-based anode materials for LIBs.

from graphite to SC to HC indicates the corresponding increase in d_{002} -spacing from 0.335 nm in graphite to (0.36–0.37 nm) in SC and (> 0.37 nm) in HC. Table 1 provides a comparison of the different properties of graphite, SC, and HC materials.

2.1. Graphite

Graphite is the most common anode material for commercial LIBs. Its usage in rechargeable cells was first suggested by Rüdorff and Hoffmann in 1938.^[35] Later, in 1976, Besenhard reported the hosting property of graphite to intercalate various guest alkali-metal ions, including Li-ions.^[36] Among various forms of graphite, natural graphite flakes and highly oriented pyrolytic graphite (HOPG) are the commonly used Li-ion intercalation graphite materials.^[37–40] Graphite is a high crystalline allotrope of graphitic carbon composed of graphene layers stacked in an ABAB (hexagonal graphite) or ABC (rhombohedra graphite) sequence bonded by van der Waals forces (Figure 2a). The graphite can reversibly intercalate Li-ions below 0.5 V vs. Li/Li⁺ and shows a maximum theoretical specific capacity of 372 mAh g⁻¹ by hosting one Li guest atom by six carbon atoms (LiC₆) under ambient conditions. In a fully lithiated state of LiC₆, the Li-atoms are distributed in-plane in the van der Waals space between every pair of graphene sheets in such a manner that it avoids the occupation of the nearest neighbour sites, and the nearest neighbouring distance is 0.43 nm. During intercalation, the half-filled P_z orbitals perpendicular to the graphene planes (π -bonds) in the graphite can accept electrons with the Li 2 s

orbitals, and the stacking order of the graphene layers shifts to AA, which is also theoretically shown by Boehm and Banerjee.^[41] Therefore, for fully lithiated graphite, the graphene layers face each other where the Li–C₆–Li–C₆ sequence along the c-direction (Figure 2a) and the interlayer space between the graphene sheets raises from ~0.34 to ~0.37 nm. As a result, a volume expansion of ~10% is observed when the full Li-ion intercalation (from C₆ to LiC₆) in graphite occurs.^[30,42] However, the *in-situ* pressure analysis in graphite/ Li_xTi₅O₁₂ (LTO) full-cell, conducted by Simon Schweieler et al.,^[36] shows that a total volume expansion of 13.2% occurs in graphite after the complete Li-ion intercalation, if the gas evolution is also taken into account. They also observed that a volume expansion of 5.9% occurred at the very initial dilute stage of Li-ion intercalation, whereas the remaining 7.3% volume expansion arose during the final two stages of the intercalation. The studies suggested that to protect the graphite anode and to maintain the long cycling stability, a limited range of 80% state of charge (SOC) of the device is suitable. Later, H Michael et al.^[44] conducted an *in-situ* electrochemical dilatometry (ECD) along with X-ray computed tomography (X-ray CT) and image-based modeling for the visual inspection of graphite during galvanostatic cycling. The dilation/contraction of graphite during charging/discharging can be monitored from the corresponding graphite thickness change measured by ECD (Figure 2b). The ECD measurement over multiple cycles shows that the graphite electrode thickness varies mainly in the initial three cycles due to the formation of Solid Electrolyte Interfaces (SEI) and the morphological changes in the electrode. The

Table 1. Comparison of physical and electrochemical properties of graphite, soft carbon (SC), and hard carbon (HC).

Materials	Graphite	Soft Carbon (SC)	Hard Carbon (HC)
Raw materials	Natural graphite	Pitch/petroleum coke	Resin/biomass/pitch/
Synthesis temperature	2500–3000 °C	500–1200 °C	< 1500 °C
Structure order	High	Medium	Low
Interlayer distance (d ₀₀₂)	~0.335 nm	0.36–0.37 nm	> 0.37 nm
True density (g cm ⁻³)	~2.26	1.90–2.10	1.4–1.8
Tap density (g cm ⁻³)	~0.965	~1.00	0.5–0.81
Compact electrode density (g cm ⁻³)	1.5–1.8	~1.2	0.9–1.0
Electrode expansion rate (%)	~10	1–10	~1
Initial Coulombic Efficiency (ICE)	Excellent	Medium	Poor
Cycling stability	Medium	Good	Excellent
Voltage profile	Low-voltage plateau	Sloping voltage	Sloping voltage + plateau voltage
Cost	Low	Medium	High
Safety	Good	Excellent	Excellent

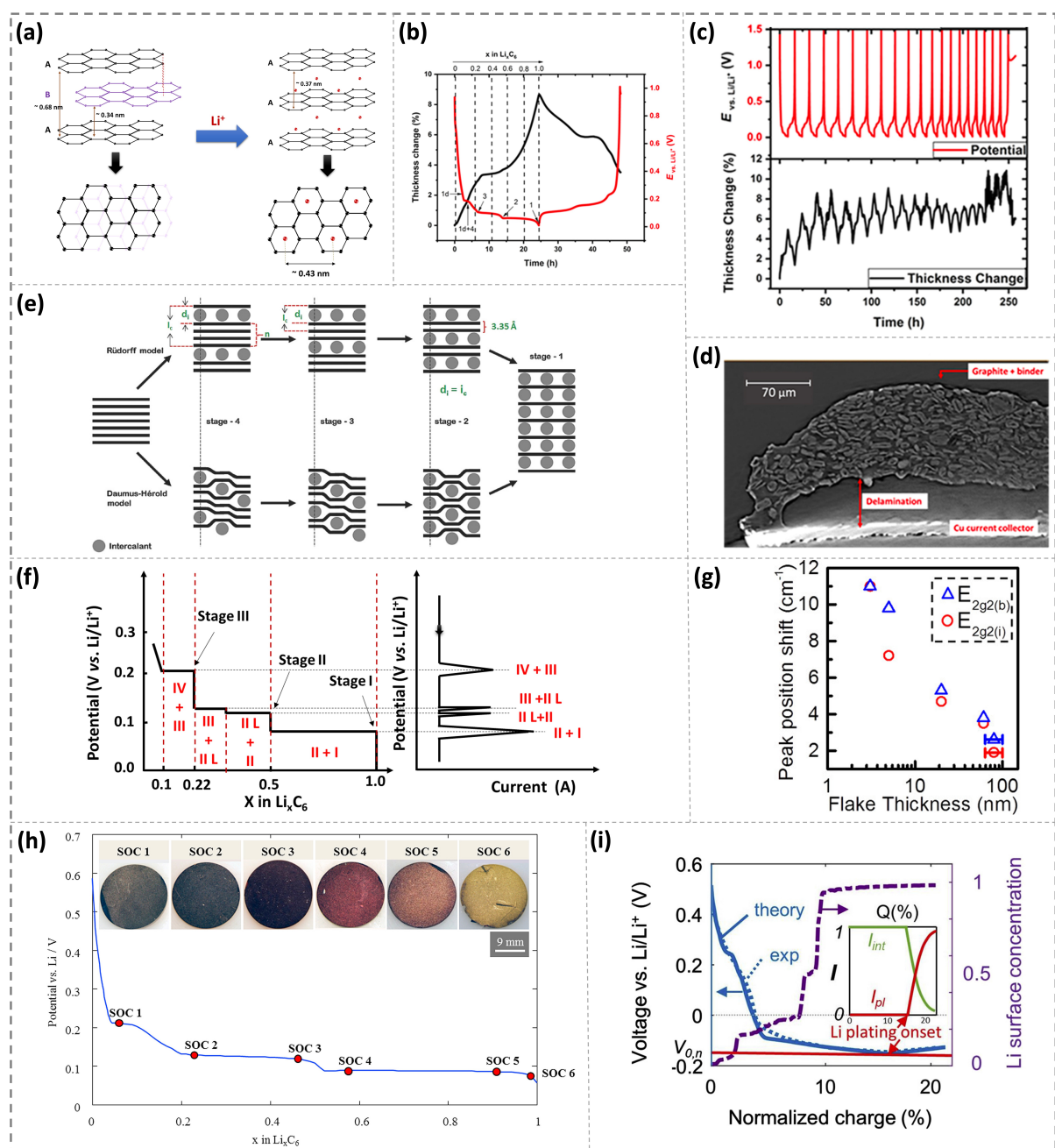


Figure 2. (a) Crystal structure of graphite with ABABA stacking of graphene layers [100]. The voltage profile with the corresponding dilation record of graphite from the *in-situ* ECD dilatometry measurement during (b) the initial cycle, (c) 20 cycles, and (d) the image acquired using X-ray CT displays the delamination occurs in the electrode after 20 cycles. Reproduced from ref.^[44] Copyright 2021, with permission from IOP Publishing Limited. (e) Representation of Li insertion stages in the graphite based on Rüdorff and Daumas-Hérould's models. Reproduced from ref.^[48] Copyright 2017, with permission from Wiley-VCH. (f) Schematic illustration of voltage profile and the corresponding cyclic voltammogram of Li-ion intercalation processes of lithium into the graphite.^[50,54] (g) Raman peak position shift of the split G band for graphite flakes at different thicknesses. Reproduced from ref.^[58] Copyright 2022, with permission from the American Chemical Society. (h) Photograph of color formation in graphite electrodes after different stages of the state of charge (SOC) indicates the degree of lithiation. Reproduced from ref.^[59] Copyright 2015, with permission from Elsevier (i) Potential and phase field model predicted Li surface concentration during lithiation shows the Li-plating onset potential when the graphite surface concentration of Li-ions exceeds 1. Reproduced from ref.^[62] Copyright 2021, with permission from Elsevier.

subsequent cycles create thickness hysteresis where the initial thickness of the electrode cannot be achieved, and the irreversible dilation over cycling leads to the electrode delamination, which is observed in X-ray CT taken after 20 cycles (Figure 2c, d).

In graphite, the intercalation is more favorable through prismatic surfaces (arm-chair and zig-zag faces) or edge planes (parallel to) other than the basal (perpendicular to) graphene plane.^[45] The computational studies to quantify the Li-ion intercalation mechanism in highly oriented pyrolytic graphite

(HOPG), conducted by K. Persson et al.,^[46] utilizing Devanathan–Stachurski electrochemical methodology with ab initio computations show that the Li-ion diffusivity is high in parallel to the graphene plane ($\sim 10^{-7}$ – $10^{-6} \text{ cm}^2 \text{ s}^{-1}$) than along the grain boundaries or perpendicular to the graphene planes ($\sim 10^{-11} \text{ cm}^2 \text{ s}^{-1}$). Further, the intercalation in graphite proceeds through different ‘stage formation’, creating Lithium–Graphite Intercalation Compounds (Li–GICs) at different stages, and each stage index, n (n = I, II, III, IV) is an indication of the number of graphene layers between two intercalant guest Li-ion layers.^[47–50] The preference for occupancy of Li-ions during the staging process highly depends on the thermodynamic phenomena related to the energy required to expand the van der Waals gap between the two graphene layers and the repulsive force between the guest ions.^[51,52] Therefore, in order to reach a more energetically stable state, the first preference of Li-ions goes to higher van der Waals gaps. Initially (above Stage IV), the concentration of Li-ions in the graphene layers is very low and proceeds through different stages, as explained by Rüdorff and Daumas–Hérolde’s models (Figure 2e).^[48,53] The staging phenomenon can be easily figured out from the galvanostatic charge-discharge profile, as the flat plateau shows the co-existence of two phases, and the corresponding current peaks can be seen in the linear potential sweep voltammetry (Figure 2f).^[50,54] These staging processes can be further confirmed by Raman spectroscopy and X-ray diffraction.^[55–57]

J. Zou et al.^[58] conducted *in situ* optical microscopy and Raman spectroscopy studies on Li-intercalation in graphite flakes, showing that the tensile strength along the graphene sheets increases while the thickness of graphitic flakes decreases. They observed a negative wavenumber Raman shift in the lower $E_{2g2(i)}$ and upper $E_{2g2(b)}$ frequency components (Figure 2g), which corresponds to the carbon atom vibrations in interior graphite layers of the split G-band during the early stages of Li-ion intercalation in thin graphite flakes indicating the weakening of the C–C bonding. This provides an insight into the larger degradation/ aging of thinner flakes of graphite (~ 1 – 7 nm – 60 nm) compared to thicker commercial microcrystalline graphite flakes with a typical thickness in the range of $\sim 100 \text{ nm}$. Since the Li-ion intercalation in graphite occurs below the reduction potential of the electrolytes, an SEI layer is formed on the surface of the graphite during the initial cycling. This decomposition starts below 1.0 V, which shows a small initial flat plateau in the voltage profile. Because of this SEI layer formation, a hysteresis is seen in the experimental curve, showing the irreversible charge loss due to the irreversible consumption of Li-ions and the decomposition of electrolytes. Moreover, there is a series of color changes in the graphite visible at different states of charge (SOC), showing a yellow color during the fully lithiated state, and the introduction of additives influences the color, sometimes changing to a golden color (Figure 2h).^[59–61] This unique change in color at different phases, due to the change in the electronic band structure because of the lattice space variation during Li-ion intercalation, helps to identify the phase separation and the Li-ion dynamics. Moreover, the transition from Li-ion intercalation to Li-plating, which commonly occurs during the fast-charging process, can

also be discerned by the color transition from gold to grey and turn to dark when the lithium is irreversibly plated or the formation of electrically isolated lithium during the Li dissolution process.^[59,62,63] T. Gao et al.^[62] elucidate the mechanism of Li-plating in highly oriented pyrolytic graphite and the transition between Li-intercalation and plating by utilizing a combination of *in situ* optical microscopy measurement along with theory and modeling. The *in situ* optical microscopy provides insights into the spatial dynamics of Li-ion insertion and plating. Meanwhile, the developed phase-field model can quantitatively describe the Li-ion concentration inside the particle, hence predicting the onset of Li-plating potential (Figure 2i).

To conclude, graphite is still the dominant anode material in LIBs, which is interesting to both industry and academic researchers owing to its high abundance, favorable tapping density, and superior electrochemical performance with minimal volume expansion (approximately 10%) in comparison to alternative conversion and alloy-type materials. However, there are many limiting factors, including low storage capacity and high-rate capability need to be addressed. Various research activities are going on to improve the electrochemical performances of graphite from different angles, including improving energy density, cycling stability rate capability, initial coulombic efficiency, and safe operating conditions. The improved energy density of graphite can be achieved through various techniques by implementing adsorption sites through porous structures,^[64] reversible formation of Li–GICs ($\text{LiC/Li}_2\text{C}_2$) through lithium plating,^[59,65,66] or by incorporating metals or metal oxides with graphite composite electrodes.^[67] The rate capability can be enhanced by facilitating the diffusion of Li-ions through the graphite structure, which could be achieved by engineering the morphology and size of the particles. Further, creating a thin and homogeneous SEI layer on the graphite electrode surface through electrolyte additives improves the initial coulombic efficiency and cycling stability. Moreover, different *in-situ* studies are required to elucidate a detailed fundamental understanding of Li-ion storage, which helps to develop novel strategies to improve the electrochemical performance of graphite.^[38,54,68–70]

2.2. Hard carbon

The non-graphitizable hard carbon (HC), first introduced as an alternative to soft carbon by Sony in their second generation LIB, is considered the most promising anode material alternative to graphitic carbons.^[32,71] It exhibits a very high reversible capacity of more than 500 mAh g^{-1} in the potential range of 0–1.5 V vs. Li/Li^+ and has better cycling stability. Hard carbon has a disordered structure with a random orientation of a few graphitic layers arranged in a short-range order, which provides many nanovoids, micropores, and carbon defective sites.^[33,33,72] Figure 3a shows the typical voltage profile of Li-ion insertion/extraction in hard carbon. The large hysteresis in the voltage profile represents its low initial coulombic efficiency (ICE) due to the high irreversible reaction happening at the initial cycle

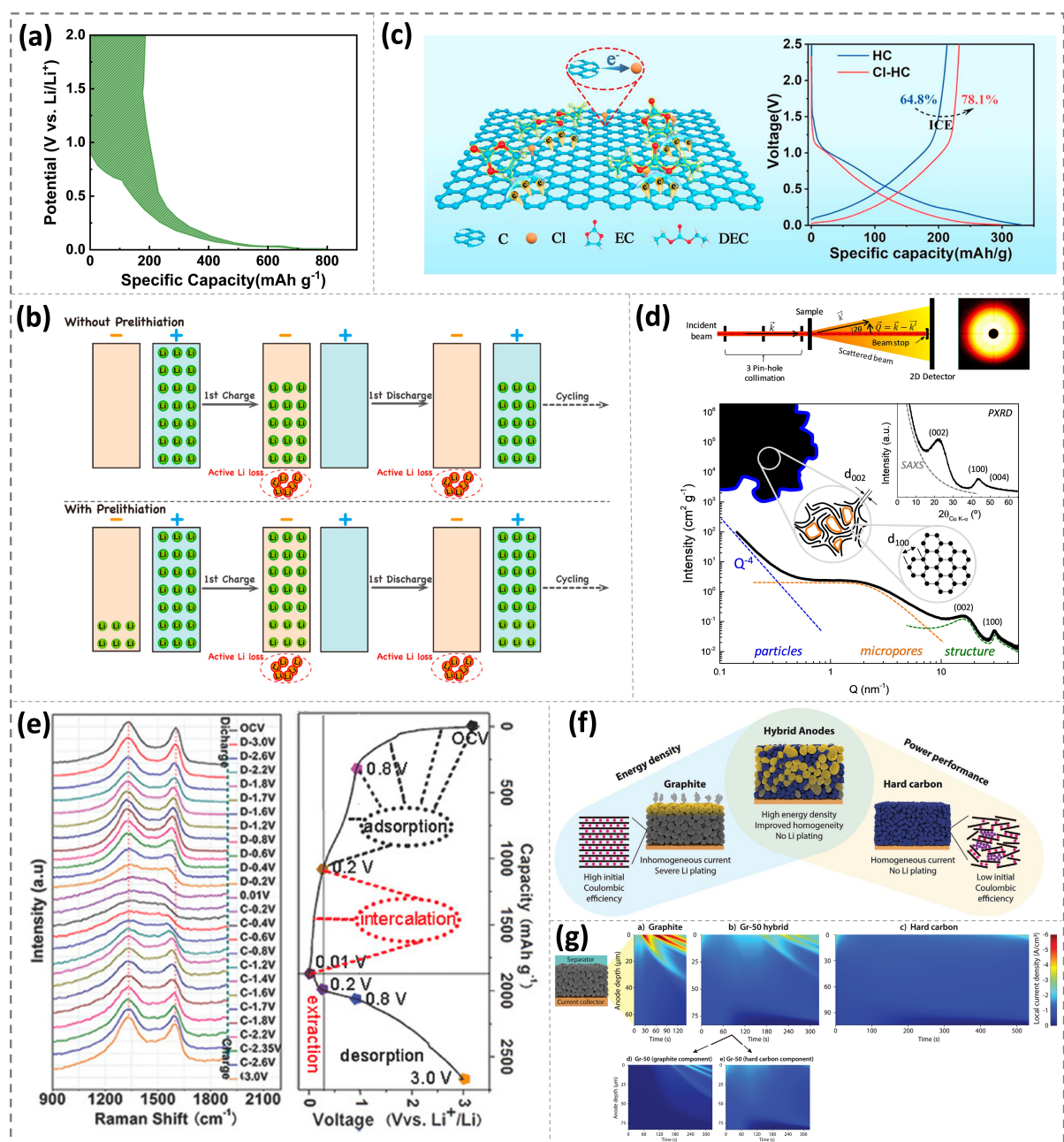


Figure 3. Voltage profile of a typical Li-ion insertion/extraction in hard carbon. (b) The schematic illustration represents the influence of pre-lithiation during the initial cycle in LIB. Reproduced from ref.^[80] Copyright 2020, with permission from the American Chemical Society. (c) Schematic illustration showing the mechanism of high ICE occurred in Cl-treated HC and the corresponding improvement shown in the voltage curve of Li//Cl-HC compared to the Li//HC half-cells at 50 mA g⁻¹. Reproduced from ref.^[81] Copyright 2021, with permission from the American Chemical Society. (d) Schematic representation of the SAXS instrument used to evaluate the microcrystalline distribution in microporous HC (Top panel) and the corresponding intensity versus scattering vector curve showing the intensity observed in the large, intermediate, and low Q ranges, along with the schematic drawing of the structural, microstructural, and morphological features respectively. The inset represents the corresponding PXRD patterns. Reproduced from ref.^[82] Copyright 2019, with permission from the Elsevier. (e) In-situ Raman spectra (left side) taken at different charge/discharge potentials (right side) during the initial cycle of N-doped HC nanoshells vs. Li/Li⁺ half cells. Reproduced from ref.^[88] Copyright 2018, with permission from the Wiley-VCH. (f) Schematic picturization of integration of graphite and carbon electrode to achieve synergistic electrochemical performance, and (g) evolution of the local reaction current density as a function of position showing homogenous current distribution in graphite, Gr-50 hybrid, and hard carbon anodes simulated by the continuum scale electrochemical simulations during 4 C charging. Reproduced from ref.^[104] Copyright 2020, with permission from the Wiley-VCH.

due to the SEI layer formation.^[73-76] Pre-lithiation is an effective strategy to improve the ICE of HC when the pre-lithiated ions compensate for the Li-ion loss that occurred during the initial irreversible SEI layer formation (Figure 3b).^[77-79] Zhang et al.^[80]

developed a fast and controllable pre-lithiation method to compensate for the initial irreversibility in hard carbon. The pre-lithiated hard carbon assembled with LiNi_{1/3}Co_{1/3}Mn_{1/3}O₂ cathode showed a high ICE of 90.2% compared with 75.5%

exhibited by the pristine hard carbon. Also, the full cell with pre-lithiated hard carbon exhibits high cycling performance with a higher capacity retention of 93.4% after 200 cycles at 1 C. N. Ren et al.^[81] demonstrate that by regulating the work function of HC, it is possible to improve the ICE significantly. The Cl-treated HC enhances the work function by transferring electrons from C to Cl, inhibiting the reduction of solvent molecules in the electrolyte, which reduces the formation of the SEI layer and hence improves the ICE of the hard carbon (Figure 3c). The non-well-stacked microcrystalline graphite structure of HC provides more Li^+ storage capacity than the well-ordered graphite structure. The small-angle X-ray scattering (SAXS) provides detailed information regarding the micro-crystalline distribution (Figure 3d).^[82] As shown, the low scattering vector (Q) value, corresponding to a slope region, indicates the particles or larger pores on the surface of HC, whereas the nanopores are represented by the shoulder region (high Q-value). It is evident that the presence of complex microstructure and pore distributions limited the diffusion of Li-ions inside the hard carbon, which negatively affected the rate capability. Also, the low tap density of hard carbon is another main drawback when considering it at the commercial level.^[75,83]

Due to the higher structural complexity of hard carbon, the Li-ion storage mechanism is still a debatable topic.^[10,84] Steven and Dahn explained the Li-ion storage inside the hard carbon by the "intercalation-adsorption" mechanism based on *ex-situ* small angle X-ray scattering (SAXS) analysis.^[85] According to them, the sloping capacity exhibited by the hard carbon is assigned to the insertion of ions between the graphitic layers, followed by the low voltage plateau capacity, which is attributed to the micropore filling.^[86,87] On the contrary, recent studies of an alternative "adsorption-intercalation" mechanism, where ion adsorption at the defect/edge sites is responsible for the high voltage sloping region followed by the intercalation of Li-ions inside the short-range ordered graphitic layers, which attributes the low voltage plateau capacity (Figure 3e).^[88] Recently, C. W. Tai et al.^[89] revealed that the closed ultramicro pores of $<0.7\text{ nm}$ in HCs can facilitate the Li-ion insertion at very low voltage without permitting the solvent molecules, thus offering higher reversible capacity by curtailing the SEI layer formation. They showed that the micropore-tuned HC with abundant ultra-micropore delivers a high reversible capacity of 550 mAh g^{-1} at 50 mA g^{-1} in a potential range of $0.001\text{--}1.5\text{ V}$, among which the 230 mAh g^{-1} capacity is provided by an ultrahigh low-voltage plateau at a very lower potential of $0.001\text{--}0.1\text{ V}$ (vs. Li^+/Li). Further, they found that the hydrogen treatment is an effective method to improve the ICE of HC by reducing the oxygen content. The various reports on HCs demonstrated that the complex microcrystalline nanotexture of HCs is highly bound with the synthesis conditions, and hence, the Li-ion storage capacity is also dependent on the nature of the synthesis of HCs. For instance, the Li-ion storage study in nano-porous hard carbons, conducted by J. Yang et al.^[90] shows that the large surface area and suitable porous texture play a major role in the accommodation and transportation of Li-ions. The kinetic studies reveal the dependence of Li-ion diffusion in hard carbon on the pore distribution. The hierarchical porous

carbons exhibit the highest capacity of 503.5 mAh g^{-1} at 0.2 C rate and a very high 5 C rate, maintaining a capacity of 332.8 mAh g^{-1} . W. Li et al.^[91] synthesized a spherical hard carbon (SHC) by one-step programmed heating of potato starch under an inert atmosphere, showing a reversible capacity of about 531 mAh g^{-1} with a first-cycle coulombic efficiency of 73.1% and also displays good rate capability (at 5 C rate, it retains a capacity of 87% to that at 0.1 C). Similarly, different types of HCs are synthesized from different sources, including resin,^[92–94] pitch,^[95,96] and various biomass such as lignin,^[97,98] starch,^[99,100] cellulose,^[101] etc. L. Xie et al. provide a detailed review of the Li-ion storage in different HCs synthesized at different conditions from various raw materials.^[32,99] Utilization of hybrid graphite/HC anodes is another strategy to achieve high-performance LIBs by merging the high energy and high ICE properties of graphite with the high power and homogeneous current distribution property of HC (Figure 3f).^[102,103] Neil P. Dasgupta's group recently showed that a mixture of graphite and HC hybrid anode achieves fast charging for LIBs up to 6 C with an energy density of $>180\text{ Wh kg}^{-1}$. This improved electrochemical performance is attributed to the increased homogenous current distribution in the anode, as substantiated by the continuum scale electrochemical simulations (Figure 3g).^[104]

In brief, HC holds promise as an alternative anode material with the potential for high capacity. However, several challenges, including low ionic conductivity, low tapping density, and Li-ion diffusion, must be addressed to enhance electrochemical performance and establish commercial viability. Various strategies, including pre-lithiation halogen functionalization of HC to enhance the work function and surface oxygen removal, appear promising for improving ionic conductivity. Furthermore, designing novel electrolyte combinations may reduce the formation of a thick solid-electrolyte interphase (SEI) layer, thereby enhancing the ICE. Moreover, it is crucial to tune the porosity, as it significantly affects the tap density of HC and the diffusion of Li-ions within the material. These factors are highly dependent on the choice of precursors and the methods employed for HC synthesis.

2.3. Soft carbon

Soft carbon (SC) is the first carbonaceous material used in the first generation Li-ion cells, which was produced from petroleum coke.^[12,105–109] It can be produced from pitch or tar or by pyrolysis of organic polymers such as polyvinyl chloride in a low-oxygen atmosphere.^[110–113] Unlike hard carbon, soft carbon, containing a semi-graphitic structure, has highly ordered graphitic domains arranged in a turbostatic disordered manner. The disordered area in soft carbon is the high-strain region, whereas the graphitic region with higher-order crystallinity is the low-strain region. These carbons in the low-strain region are responsible for the high electronic conductivity of soft carbon.^[11,114–116] Therefore, as an anode material for LIBs, soft carbon exhibits an excellent rate of performance.^[117–119] Recently, A. Pendashteh et al.^[112] proposed a facile strategy to synthesize SC with reduced particle size by performing the

mechanical treatment (ball milling) during the intermediate stage of the pyrolysis, showing better electrochemical performance (in terms of improved ICE, high energy and power density) compared to the SC synthesized by the traditional route (Figure 4a). Generally, soft carbon exhibits a sloping potential profile similar to hard carbon but without a low voltage plateau (Figure 4b).^[111,120] It has been found that the Li-ion insertion in SCs is highly dependent on the heat-treatment temperature (HTT) during the synthesis. Basically, the low-temperature heat-treated SC undergoes three types of Li-ion insertion mechanisms: (a) the adsorption or partial charge transfer of Li-ions on the hexagonal surface or on unstacked carbon layers, which occurs in the potential window of 0.25 to 0.8 V (represented as Type I), (b) intercalation of Li-ions into the carbon layers during charging and discharging in the potential window of 0.0 to 0.25 V (represented as Type II), and (c) the insertion of Li-ion to the microspaces at the carbon cluster edges which occurs at very low potential (represented as Type III) (Figure 4c). I. Mochida et al.^[121] found that in the low HTT synthesized SC, the Li-ion storage is profoundly contributed by the irreversible Type III mechanism, which results in lower ICE (Figure 4d, e). Among the reversible Type I and Type II mechanisms, the capacity due to the Type II mechanism increases with HTT due to the increased graphitized carbon, whereas the capacity due to Type I is also reduced with increased HTT because of the less available free surface of the hexagonal sheet due to the increased graphitization. However, in contrast to the staged Li-intercalation mechanism in graphite (Figure 2f), no staged Li-insertion/extraction is present in the SC, which is verified through *in-situ* XRD measurements (Figure 4f) conducted by M. Schroeder et al.^[117] This no-staging Li-insertion process can also be discerned from the galvanostatic intermittent titration techniques (GITT) measurements, where no sharp fall in diffusion coefficient was observed in SC compared to the graphite (Figure 4g). The sloped voltage profile of SC and their high-rate capability compared to graphite (Figure 4h) demonstrates the potential of SC to be utilized as anode materials for high-power applications. The high cycling stability exhibited by the high-power Li-ion capacitors (LICs) fabricated with SC as anode indicates the potential of SC to withstand numerous charge/discharge cycles without significant capacity degradation.^[118,119]

In summary, soft carbon can be considered in the high-power Li-ion storage material category, boasting superior conductivity and rate capability when compared to hard carbon. It also demonstrates a higher Li-ion storage capacity compared to graphite. However, addressing the significant initial coulombic loss remains a primary challenge.

In conclusion, graphite, HC, and SC are the Li-ion storage carbonaceous anode materials in the bulk format, and their storage mechanism largely depends upon the structural order. In general, the specific capacity of the materials increases when the structural disorder rises, as it is visible from graphite to SC to HC. Also, the increase in structural disorder decreases the electrode expansion rate, which positively affects the cycling stability. However, the ICE shows decreasing while increasing the defects in the material structure, which has a negative

impact on cycling stability. Hence, choosing appropriate carbon anodes necessitates balancing energy density and the ICE. Moreover, in commercial considerations, factors such as tap density, safety, and cost-effectiveness need to be taken into account when selecting these carbon bulk materials as anodes for LIBs.

2.4. Nanocarbons for LIBs

The emergence of nanoscience and nanotechnology revolutionized the material engineering area, which provides more opportunities for various materials to exhibit anomalous electrochemical properties that are impotent in their bulk form.^[10,122] Also, it avoids volumetric expansion during lithiation and improves the capacity of storing charges volumetrically with high elasticity and mechanical strength. The carbon in the nano dimension provides the advantage of high surface area that enhances the wetting of electrolytes, which reduces the Li-ion diffusion length and, hence the diffusion time. At lower dimensions, the carbon exhibits a different Li-ion insertion mechanism compared to its bulk counterpart and shows superior electrochemical properties, which are highly influenced by their morphology. However, the presence of high surface area and defects initiates a large amount of electrolyte dissociation during the initial lithiation, forming a passive SEI layer at the electrode/electrolyte interfaces, which consumes a substantial amount of electrolytes and leads to very little ICES.

2.4.1. Graphene

Graphene, the mother of all graphitic forms discovered in 2004,^[123] is virtually a single-layer, two-dimensional cut of graphite, where the SP² hybridized carbon atoms are arranged in a hexagonal honeycomb lattice. The theoretically high surface area ($\sim 2600 \text{ m}^2 \text{ g}^{-1}$), large charge carrier mobility ($\approx 2,00,000 \text{ cm}^2 \text{ V}^{-1} \text{ s}^{-1}$), high electronic mobility (10,000 $\text{cm}^2 \text{ V}^{-1} \text{ s}$), high thermal ($\approx 5000 \text{ W mK}^{-1}$) and mechanical ($\approx 130 \text{ GPa}$) conductivity of graphene holds special attention as anode material for LIBs.^[48,124] The graphene layer can accommodate two times more Li-ions than that of conventional graphite, as first suggested by Dahn et al.^[115] Unlike the Li-ion intercalation (staging mechanism) in graphite, the graphene layers can host Li-ions on both sides through adsorption at lower potentials ($< 0.5 \text{ V}$ vs Li/Li⁺). Theoretically, graphene shows a specific capacity of $\sim 744 \text{ mAh g}^{-1}$, corresponding to a stoichiometry of Li_2C_6 , which is double the specific capacity exhibited by the graphite (372 mAh g^{-1} , LiC_6). However, in practical, graphene anodes report a high specific capacity ranging from 790–1050 mAh g^{-1} , which is due to the additional Li-ion storages at the edges sites or other defects that act as active sites for Li-ions.^[125–127] However, the single-layer graphene developed by the chemical vapor deposition (CVD) method on copper foil shows limited Li-ion storing capacity due to the lower binding energy of lithium to the carbon and the repulsion between the Li-ions on both sides of the graphene layer

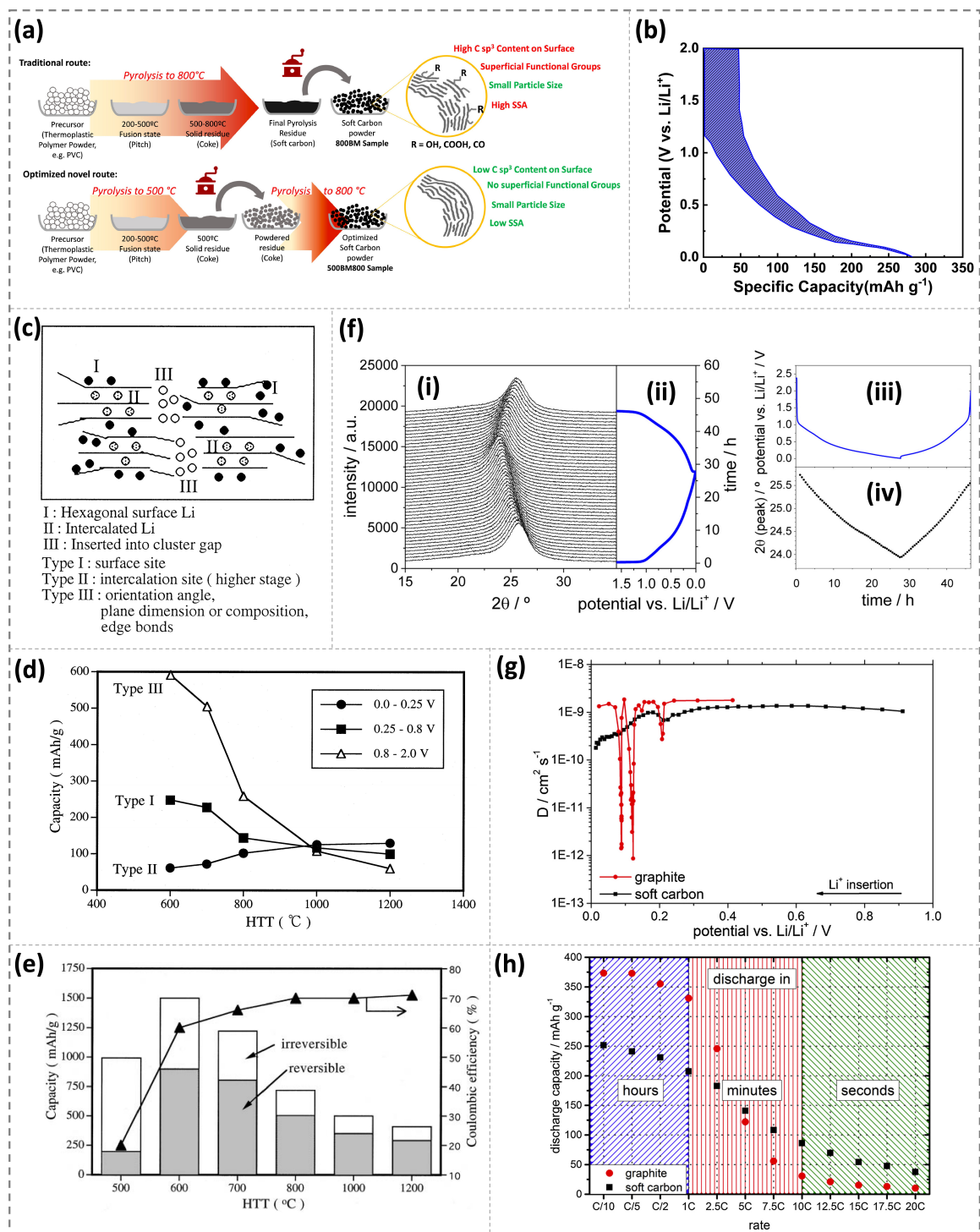


Figure 4. (a) Schematic representation of soft carbon (SC) on synthesis from the traditional route (top) and optimized mechanical ball milling treatment (bottom) during the preparation. Reproduced from ref.^[112] Copyright 2022, with permission from the Elsevier. (b) Voltage profile of a typical Li-ion insertion/extraction in soft carbon (c) Schematic representation of Li-ion insertion model into the SC synthesized at low temperature. The contribution of discharge capacity (d) in different types, divided based on the potential range, and (e) the reversible and irreversible contribution along with the coulombic efficiency (%) in the initial cycle of the SCs synthesized at different temperatures. Reproduced from ref.^[121] Copyright 1998, with permission from the Elsevier. (f) (i) In-situ XRD spectra taken at different lithium insertion/extraction potentials in PeC derived SC, (i, ii, and iii) along with the corresponding 2θ position of the (002) diffraction peak vs. time (iv). (g) Comparison of diffusion coefficient at different Li-ion insertion potentials calculated from the GITT measurements of graphite and soft carbon-based anodes, and (h) the rate capability C-rate test of graphite and soft carbon-based anodes in a potential window of 0 to 1.5 V vs. Li/Li⁺. Reproduced from ref.^[117] Copyright 2014, with permission from the Elsevier.

covering only 5% of the graphene surface.^[128] This is theoretically substantiated by the positive Li-ion absorption energy on the surface of defect-free single-layer graphene (SLG) for the entire range of Li-ion content calculated using the cluster expansion method and density functional theory (Figure 5a).^[129] Further, studies into few-layer graphene (FLG) show that the Li-ion intercalation is stronger in bilayer graphene while increasing the graphene layers (*n*) converges the Li-ion intercalation like the bulk graphite. However, for higher Li-content, the bulk graphite shows stronger Li-ion intercalation than the FLGs (Figure 5b). This unique bilayer property can be attributed to the presence of two exterior graphene layers around the Li-ions, whereas for FLGs, at least one interior graphene layer will be present, where the Li-bonding with the interior graphene layers is weak due to the repulsion of Li-ions from both sides of the interior layers.

M. Kühne et al.^[130] utilized time-dependent Hall measurements to probe the in-plane Li-ion chemical diffusion coefficients in bilayer graphene, which is found to be higher ($7 \times 10^{-5} \text{ cm}^2 \text{ s}^{-1}$) than the in-plane Li-ion diffusion in the bulk graphite.^[46,131,132] The same group investigates the Li-ion intercalation in bilayer graphene by utilizing an *in-situ* low-voltage transmission electron microscopy, revealing that the Li-atoms undergo multi-layered close-packed superdense phase order between the two graphene layers.^[133] Further, the activation energy calculation of in-plane Li-ion diffusion in the bilayer graphene sheets shows facile diffusion of Li atoms within the close-packed Li phase. Moreover, an alternative path is also offered for Li-ions to diffuse through the outside of the bilayer graphene followed by vertical diffusion through the defects, making Li-ions access any place between the bilayer graphene system. Detailed Li-ion intercalation process in freestanding bilayer graphene foam (Figure 5c) conducted by K. Ji et al.^[134] demonstrated that the intercalation happened only inside the layer and introduced a new Li-storage planar model in 2D bilayer graphene (Figure 5d). Also, they found that the Li-intercalation occurs through a four-time fractal way irrespective of the type of graphene (bilayer graphene to bulk graphite) until the LiC₆ saturated composite occurs. Recently, D. W. Kim et al.^[135] revealed the reason for excess Li-ion storage beyond LiC₆ in graphene structures at the reduced dimensional scale (RDS). They found that the synergetic energy storage exhibited by the RDS graphene with the porous structures is due to the cumulative edge and surface effects as well as defects like Stone-Wales defect (SW), line defect (LD), and divacancy defect (DV) opens additional rooms for Li-ion accumulation, which escalates the capacity beyond the conventional limited LiC₆ intercalation. The developed RDS graphene with open-porous structures exhibited exceptional reversible Li-ion storage capacity (3074 mAh g⁻¹) with 163% capacity elevation after 2000 cycles at 5 C (Figure 5e). From the above studies, it is obvious that the amount of Li-ion stored by graphene is highly dependent on the nature of the synthesized materials.

Reduced graphene oxide (RGO) is the most reported anode material for LIBs, as most of the bulk preparation is based on chemical solution processes.^[126,136,137] However, one of the main drawbacks of RGO-based anode is its low ICE. Even though a

very high capacity of $>2000 \text{ mAh g}^{-1}$ is reported for RGO during its initial discharge, a very low de-insertion is happening. This massive irreversible reaction in the initial cycle is due to the high electrolyte decomposition because of its high specific surface area (SSA), forming a passive SEI layer. Also, over repeatable cycling, the reduction of oxygen-containing groups on the surface of RGO leads to graphene layer re-stacking, which causes a reduction in reversible capacity compared to graphene.^[138] However recently, there have been some reports showing improved electrochemical performance of graphene by introducing doping or making porosity. For instance, an *in-situ* fabrication of doped hierarchically porous graphene (DHPG) electrodes designed by Wang et al.^[139] shows an ultrafast Li-ion storage property and exhibits a very long cycling stability of 3000 cycles at 5.0 A g⁻¹.

Different morphological engineering of graphene such as porous graphene,^[135,140–150] holey graphene,^[151–157] defective graphene,^[158–163] graphene spheres,^[164–168] graphene nanoribbons,^[169–177] etc., have been conducted with the aim of enhancing the Li-ion storage capacity and rate capability owing to the improved surface area, generated active surfaces, and increased diffusion channels. Further, developing graphene derivatives through heteroatom doping,^[178–191] covalent functionalization,^[192–196] homogenous mixing with other compounds,^[189–192] etc., are different strategies to achieve high electrochemical performances. Moreover, graphene is an excellent material for developing free-standing, flexible electrodes, which is required for developing wearable and implantable energy storage devices.^[201–206] A detailed discussion of the different graphene anodes and their electrochemical properties was recently reviewed by J. Bi et al.^[207] which is out of the scope of the current review.

To summarize, graphene presents significant potential as a promising anode material, serving as an alternative to graphite for the next generation of LIBs. This is attributed to the remarkable advantages of graphene over commercial graphite, encompassing the freedom for chemical, surface, and morphological engineering, as well as hetero-atom doping. Furthermore, graphene provides the opportunity to create flexible and free-standing electrodes, thereby lowering the cost and weight of LIBs, and also opens avenues for the advancement of wearables and flexible electronic gadgets.^[208,209] However, despite the significant benefits and notable progress in graphene in recent years, numerous challenges, including lower initial coulombic efficiency, large voltage hysteresis, low tapping density, etc., must be addressed. Additionally, the re-stacking issue of graphene during bulk synthesis remains a concern for large-scale applications.

2.4.2. Carbon Nanotubes (CNTs)

Carbon nanotubes (CNTs), an allotrope of graphite, are structurally conceptualized as the wrapping of graphene sheets in a one-dimensional cylindrical tubular form with fullerene (C₆₀) caps.^[210,211] Generally, CNTs are of two types: Single-walled carbon nanotubes (SWCNTs) and multi-walled carbon nano-

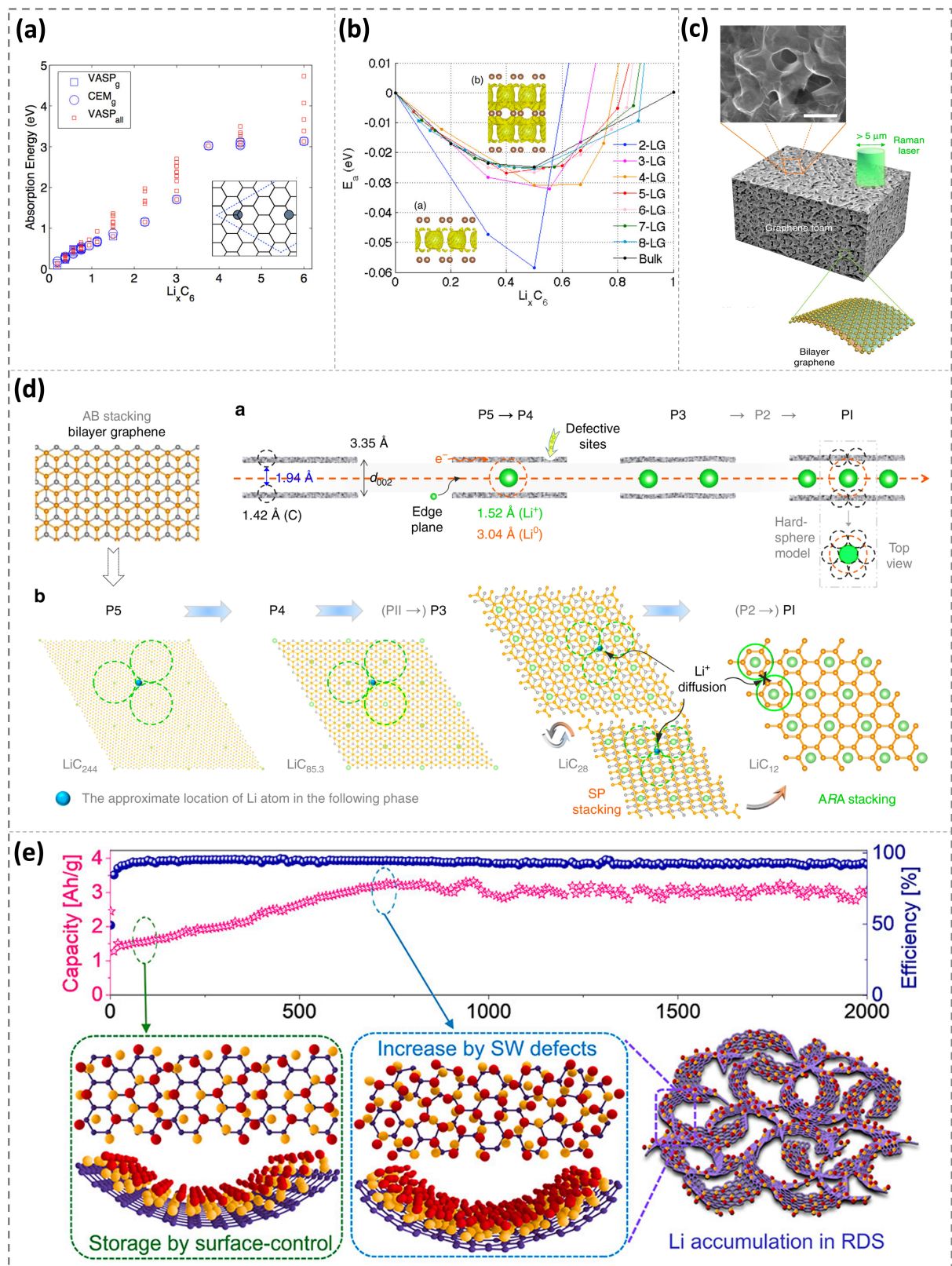


Figure 5. (a) Absorption energy in defect-free single-layer graphene predicted by the DFT calculations and the cluster expansion method as a function of Li content, and (b) graph showing the Li-ion intercalation energy simulated in few-layer graphene to bulk graphite. Reproduced from ref.^[129] Copyright 2012, with permission from the American Chemical Society. (c) Image of 3D porous morphology of bilayer graphene foam along with SEM image, and (d) schematic representation of Li-intercalation in bi-layer graphene (a, top) and the evolution of Li-distribution in the interlayer of bilayer graphene at different phases P (b, bottom). Reproduced from ref.^[134] Copyright 2019, with permission from the Springer Nature. (e) The cycling stability of RDS porous graphene with Li-metal cycled at a high rate of 5 C shows an escalation in the specific capacity over cycling (top), and the corresponding schematic represented the Li-storage mechanism emphasizes the influence of SW defect (bottom). Reproduced from ref.^[135] Copyright 2020, with permission from the American Chemical Society.

tubes (MWCNTs). The SWCNTs have diameters ranging from ~0.4 to 3 nm, showing a high conductivity of 10^6 Sm^{-1} at 300 K. On the other hand, MWCNTs contain concentric layers that are spaced 0.34 nm apart, with a diameter in the range of ~2 to 100 nm, exhibiting a high conductivity of $>105 \text{ Sm}^{-1}$. Apart from this, the CNTs have high tensile strength (up to 60 GPa), high rigidity (Young's modulus of the order of 1 TPa), and low density.^[211–216] The unique electrical, physical, and electrochemical properties make CNTs an attractive anode material for LIBs.^[217–222] Additionally, CNTs have the capability to create conductive free-standing electrodes. This offers the advantage of developing devices without the need for a current collector, significantly reducing device weight. Further, the use of free-standing electrodes made of CNTs or CNT composites is particularly advantageous in the development of flexible energy storage devices for wearable applications.^[223,224]

The Li-ion storage in CNTs varies depending on their structure and morphologies, and the insertion level of Li-ions is no longer limited to LiC_6 .^[225–227] The SWCNTs exhibit a reversible specific capacity in the range of 300 to 600 mAhg⁻¹, and MWCNTs have a capacity range of about 450 to 600 mAhg⁻¹. Numerous theoretical studies indicate that, although CNTs can store Li-ions both inside and outside the tube, the external positions are slightly more favorable for Li-ions. When considering two Li-ions within a SWCNT, the more stable configuration involves placing both ions outside. Additionally, the binding energy is highly dependent on the positions of the Li-ions.^[229–233] Further, the adsorption of Li-ions is found to be more favorable near the locations of the defects than in a defect-free nanotube, as reported by S. A. Sozykin et al.^[234] by using the first-principles modeling to study the lithium adsorption on SWCNTs with divacancy defects (2 V defect). Compared to SWCNT, the MWCNT has the potential for intercalation/de-intercalation of Li- ions significantly, similar to that of disordered carbon. The ab initio simulation studies suggested that the insertion of Li-ion through the side walls of the pristine nanotube or closed fullerene cap is energetically unfavorable (forbidden) and can only diffuse through the open ends of nanotubes. Otherwise, there should be some structural defects (topological defects containing at least nine-sided rings) that can open the path for Li-ions.^[225,232] The Li-ion adsorption in SWCNT is an endothermic process, which the defect sites can highly influence. If the defect formation energy is larger along with the increase in the defective ring on the surface of the SWCNT, the Li-ions possess less energy barrier, then the Li-ion diffusion becomes more feasible, and the peak position of the barrier shifts toward the center of the SWCNT (Figure 6a). The barrier height for the Li-ion diffusion decreases from about 24.0 to 2.0 eV with the increasing ring size of the wall from pentagon to octagon. The change in diameter of the CNTs also influences the adsorption energies of the internal and external sites. If the nanotube diameter increases to more than 0.824 nm, both the outside and internal adsorption energies become similar.^[233,235] From the analysis of electrochemical Li-ion storage properties of metallic and semiconducting SWCNTs, it is found that the metallic SWCNTs can store Li-ions five times better than the semiconducting SWCNTs as reported by S. Kawasaki et al.^[236] In

MWCNTs, the Li-ion has the option to intercalate at the interstitial spaces between the coaxial nanotubes, exhibiting higher capacity.^[237–239] However, it undergoes very high irreversible capacity and hence low coulombic efficiency in the initial cycle. Many post-synthesis approaches, such as ball milling,^[240] cutting processes,^[239] acid oxidation,^[241] etc., have been developed to mitigate the irreversibility and improve the coulombic efficiency. Doping of CNTs with heteroatoms is an effective method to improve the electrochemical storage of Li-ions.^[242–244] The Nitrogen-doped (N-doped) CNTs display higher reversible capacity as well as rate capability compared to the pristine CNTs.^[245–247] The N-doping in CNTs creates more active sites for Li-ion absorption and provides better electrolyte wettability, which enhances the electrochemical properties. Moreover, the N-doping improves the electronic conductivity of CNTs as the nitrogen contains five valence electrons, and due to its high electronegativity, it withdraws electrons from the covalently bonded carbon atoms while bonding with carbon atoms.^[248] W. H. Shin et al.^[245] developed the N-doped CNTs (NCNTs) through the plasma-enhanced chemical vapor deposition (PECVD) process, exhibiting an improved Li-storage capacity, where the Li-ions utilized the interwall space, which is confirmed by the increased interwall spacing (3.4 to 3.7 Å) observed through the HRTEM images and also an increase in wall thickness observed (15.7 to 17.8 nm) after full the lithiation (Figure 6b (i)). The increasing specific capacity in NCNT over successive cycling compared to the pristine CNT is attributed to the diffusion of Li-ions into the inner tubes through the defects created by N-doping (Figure 6b (ii)). Nitrogenation in CNTs can be considered in four different ways.^[249] First is the direct substitution of nitrogen atoms, which can significantly enhance the state density at the vicinity of the Fermi level. Second is the pyridine-like nitrogenation, which can shorten the energy band gap of semiconducting (10,0) nanotubes of 0.7 eV band gap into <0.2 eV. Third and fourth are the exohedral chemisorption of N adatoms and sidewall covalent $-\text{NH}_2$ functionalization, respectively, as both processes will convert the semiconducting (10,0) nanotubes 0.7 eV band gap into metallic. In short, the N-doping improves the electrochemical performance of CNTs as anode material for LIBs.^[250,251]

There are several issues that need to be addressed before considering CNTs as an alternative to graphite-based anodes. Unlike graphite electrodes, CNTs do not exhibit a flat Li-ion intercalation potential; instead, they display broad voltage changes during discharge. This is not suitable for most electronics that require stable voltage sources. Further, it possesses high irreversible capacity as well as large hysteresis of the voltage window and depends on the morphology of the materials. Moreover, during CNT synthesis, precise control over morphological things such as the number of layers, diameter, and length is required, and during the electrode fabrication processes such as purification, stability in CNT dispersion, post-treatments, etc., needed to be refined.

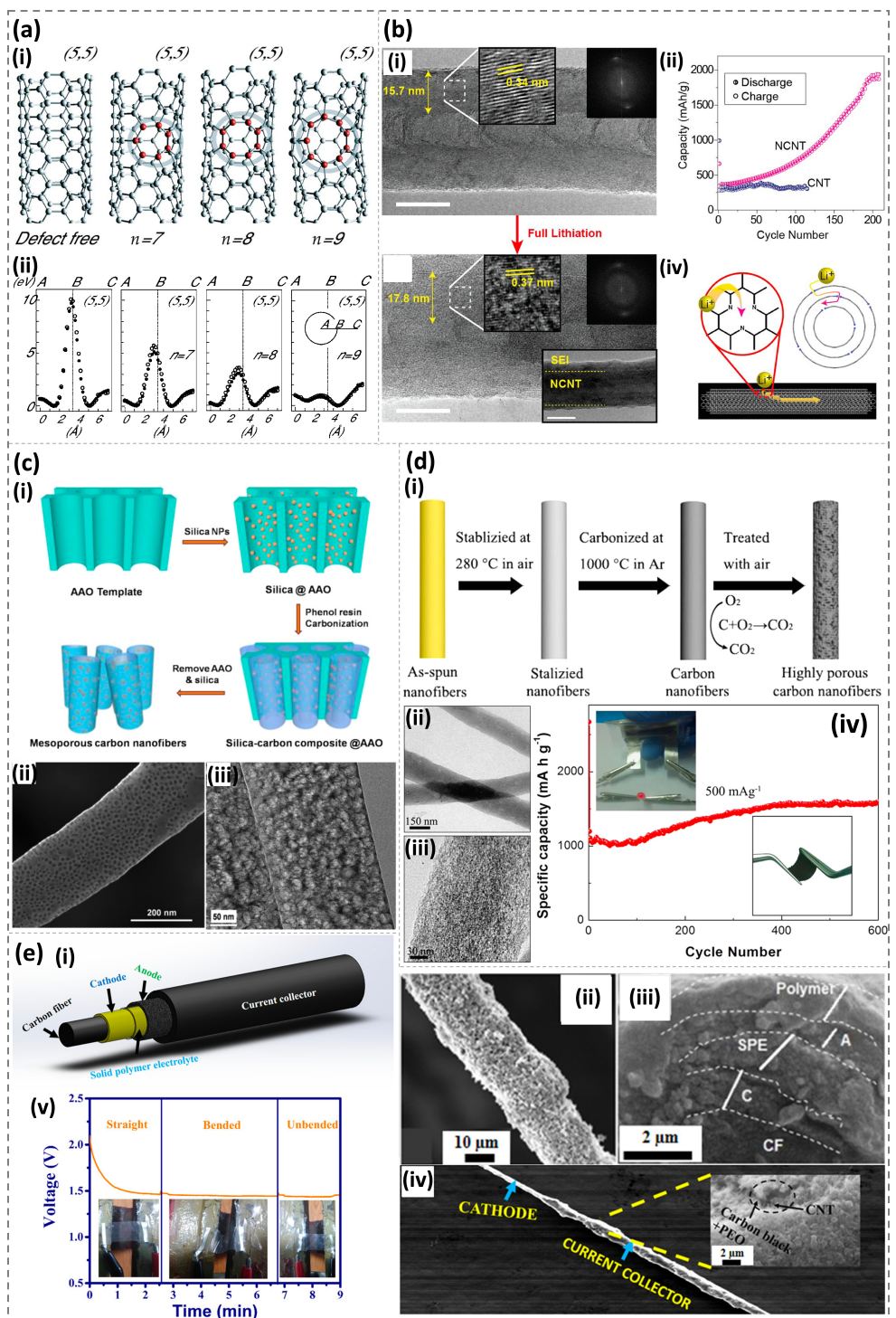


Figure 6. (a) (i) Fully relaxed (5,5) SWNT structures with defect-free and the defective simulated by the generalized-gradient approximation (GGA) calculations, and (ii) the corresponding energetics of Li-ion diffusion pathways from center represented as A to surface B to near the surface C, where the energy is considered as zero at the most stable point. Reproduced from ref.^[23] Copyright 2005, with permission from the American Physical Society. (b) (i) TEM image showing the changes in the lattice space and the interwall space of NCNT during Li-ion intercalation, (ii) increased specific capacity over cycling in NCNT compared to the commercial multiwall CNTs, and (iii) the schematic representation of the corresponding Li-ion insertion mechanism into the interwall space as well as in the NCNTs. Reproduced from ref.^[24] Copyright 2012, with permission from the American Chemical Society. (c) (i) Schematic diagram representing the synthesis of MCNFs with silica nanoparticles (NPs) on AAO=anodic aluminum oxide, (ii) and (iii) shows the low and HRTEM image for the MCNFs. Reproduced from ref.^[25] Copyright 2014, with permission from the American Chemical Society. (d) (i) Schematic diagram representing the preparation method of HPCNFs electrode. (ii) Low and (iii) high-resolution SEM images of the synthesized HPCNFs, and (iv) displays the cycling stability of freestanding flexible HPCNF electrodes. Reproduced from ref.^[26] Copyright 2015, with permission from Elsevier (e) (i) Schematic representation of LIB fiber, SEM images of the (ii) battery fiber, and (iii) their cross-sectional view coated at 120 V where A and C represent anode and cathode, respectively, and (iv) the battery fiber after the current collector deposition. (v) The unaltering voltage discharge profile of the single-battery fiber during mechanical bend testing. Reproduced from ref.^[28] Copyright 2019, with permission from the American Chemical Society.

2.4.3. Carbon Nanofibers (CNFs)

Carbon nanofibers (CNFs) are the tubular one-dimensional structure of sp^2 -hybridized carbonaceous materials having high electrical conductivity along the longitudinal direction.^[252–254] The improved surface-to-volume ratio at the electrode-electrolyte interface enhances electrolyte wettability and facilitates ionic transport by reducing the ionic transport length, making it a promising anode material for Li-ion batteries.^[255–259] Various strategies such as catalytic chemical vapor deposition (CVD) growth, electrospinning, template-based synthesis, and biomass methods are used for the synthesis of CNFs.^[252,258,260–264] Among this, electrospinning is a simple, versatile, cost-effective, and feasible method that has been extensively used for fabricating long and continuous nanofibers.^[264–271] The physical and chemical properties of CNFs are highly influenced by the chemical structures of natural and synthetic carbon precursors, including polyacrylonitrile (PAN), polyvinyl alcohol (PVA), polyvinyl pyrrolidone (PVP), poly (ethylene oxide) (PEO), cellulose, etc., utilized during the synthesis.

The first usage of CNFs as anode material for LIBs dates back to the mid-2000s. Kim et al.^[264] synthesized a high-purity carbon nanofiber web by electrospinning the polymer PAN, followed by thermal treatment in an inert atmosphere. The CNF electrode, having a high surface area and high electronic as well as ionic conductivity, exhibits a high reversible capacity (ca. 450 mAh g^{-1}) and a high-rate capability (350 mAh g^{-1} at a charge current of 100 mA g^{-1}). Introducing porosity in the CNFs creates an ultra-high surface area, which provides more charge transfer and enhances the electrochemical performance, such as high reversible specific capacity and good cycle stability compared with nonporous CNFs with similar diameters.^[272–275] The diameters of these types of synthesized porous CNFs can range from tens of nanometers to several micrometers. Many strategies such as catalytic chemical vapor deposition growth, template-based and activation strategies have been explored to control the porous structure in CNFs. Ji et al.^[273] prepared porous CNFs having a relatively large surface area of about $235 \text{ m}^2 \text{ g}^{-1}$ by the electrospinning of bicomponent polyacrylonitrile and poly-lactic acid polymer solution, followed by thermal treatments under different atmospheres. Due to the large surface area and the numerous active sites for adsorption and facile Li-ion diffusion pathways, the synthesized porous CNF exhibits specific reversible capacities of about 566 mAh g^{-1} at the first cycle and 435 mAh g^{-1} at the 50th cycle and shows stable cycling performance than non-porous CNFs. The mesoporous carbon nanofibers (MCNFs) synthesized by Xing et al.^[275] with porous anodic aluminum oxide (AAO) membrane and colloidal silica Ludox TM-40 as the dual hard templates and phenol resin as the carbon precursor (Figure 6c), achieve a very high specific capacity of ca. 1279 mAh g^{-1} and the coulombic efficiency increases to 95% within first few charge-discharge cycles. By controlling the size of colloidal silica or other mesopore agents (porogens), it is possible to vary the size and distribution of macropores/mesopores in MCNFs. W-Li et al.^[276] developed flexible, highly porous carbon nanofibers (HPCNFs) through electrospinning and utilized them as flexible and self-

supported electrodes for LIBs. The highly porous nature of HPCNFs provides highly active surface areas as well as good wetting of electrolytes and reduced contact resistance due to the 3D interconnecting networks between the numerous micro/mesopores, resulting in excellent capacity with very long cycling stability (Figure 6d). Among the heteroatom doping of carbonaceous materials, as explained earlier, nitrogen doping is the best way to enhance the lithium storage capacity. The increase in electronic conductivity while doping due to the n-type inducing nature of nitrogen introduces donor states near the Fermi level and creates more defect sites for lithium storage.^[184] Thus the CNFs with nitrogen doping also show higher reversible capacity as compared to the pristine CNFs. Wang et al.^[277] showed the nitrogen-doped carbon nanofiber webs (N-CNFWs), which are prepared by direct pyrolyzation of polypyrrole (PPy) nanofiber webs at 600°C , achieve a reversible capacity of up to 668 mAh g^{-1} at a current density of 0.1 A g^{-1} and a specific capacity of 238 mAh g^{-1} at a higher current density of 5 A g^{-1} . The nitrogen-doped porous carbon nanofiber networks (NPCNFs) synthesized by Nan et al.^[278] exhibit an ultrahigh capacity of 1323 mAh g^{-1} in the first cycle at 50 mA g^{-1} and maintain a capacity of 473 mAh g^{-1} at higher current rates (1000 mA g^{-1}). Zhang et al.^[252] revealed that the structure in CNFs is changing the Li-ions storage capacity, and the defects induced by nitrogen functionalization or doping act as host sites for Li-ions other than its storage space between the graphene layers. Chen et al.^[279] introduced an innovative synthesis method for the controlled Ni-diffusion graphitization to produce polymer-based graphitic carbon nanofibers. In this approach, Ni nanoparticles diffuse from graphitic carbon spheres into N-doped amorphous carbon nanofibers, inducing the transformation of amorphous carbon nanofibers into graphitic carbon nanofibers and generating a hollow-tunnel structure within electrospun carbon/Ni nanofibers. Following chemical activation and acid treatment, they obtain activated N-doped hollow-tunneled graphitic carbon nanofibers (ANHTGCNs). The ANHTGCNs, having a high surface area and porous structure, exhibit a high reversible specific capacity of $\sim 1560 \text{ mAh g}^{-1}$ and a remarkable volumetric capacity of $\sim 1.8 \text{ Ah cm}^{-3}$ at a current density of 0.1 A g^{-1} . From different studies, it is well understood that the electrochemical properties of CNFs are highly influenced by the precursors and the synthesis techniques.

Moreover, CNFs can be utilized in combination with other active materials to improve their Li-storage capacity and escalate the rate capability and cycling stability by providing the option of engineering the morphology, interfaces, and electronic structure.^[279–283] Further, CNFs are helping to develop flexible LIB architecture with 1D and 2D structures.^[270,271,281,284–287] For instance, A. Yadav et al.^[288] showed a facile strategy to develop flexible micro ($\sim 22 \mu\text{m}$) coaxial solid-state LIBs on CNFs by utilizing electrophoretic deposition and dip-coating methods (Figure 6e). The LTO/LFP-based single-fiber flexible micro-LIB delivers an aerial discharge capacity of $4.2 \mu\text{A h cm}^{-2}$ at a current density of $13 \mu\text{A cm}^{-2}$ and exhibits excellent cyclic performance with 85% retention of capacity after 100 cycles without harming the device performance while bending.

In summary, akin to CNTs, CNFs also experience a challenge of high initial irreversible capacity with a broad discharge voltage. Nevertheless, the advantageous feasibility of the electrospinning technique and the cost-effective mass production of CNFs set them apart as a significant advantage over CNTs. C. Sun et al.^[289] reported a detailed overview of different aspects of the CNFs, including various synthesis strategies, architectural design of self-supported flexible CNFs in composition with other materials, and their applications in different energy storage devices.

2.4.4. Carbon-based composites

While comparing with the Li-ion storage mechanisms of materials that undergo alloy/de-alloy processes (e.g., Si, Ge, Sn, and SnO_2) or conversion processes (e.g., transition-metal compounds such as oxides, phosphides, sulfides, and nitrides), the intercalation-based carbonaceous materials display lesser reversible capacities.^[99,195,243,290–294] However, the pristine usage of alloy/conversion kind of materials as anodes for LIBs in real applications is not suitable due to many reasons, such as large capacity fading, poor cycling stability, large volume change, unsuitability at higher c-rates due to their relatively low electronic and ionic conductivities, and also possess unstable SEI layer formation.^[6,125,292,295,296] At this moment, the fusion of these materials with carbon matrixes (1D, 2D, and 3D carbon structures) provides good conductivity, and the carbon materials also act as a strain buffer to confine the volume changes of the host materials. Moreover, the carbon-based compound with different morphologies not only provides a high surface area but also opens ionic channels between the host materials for the facile movement of charges. Thus, carbon-based composites can exhibit both high energy density and power density with improved cycle life.^[197,198,297–307]

As we know, silicon is one of the most investigated high-capacity anode materials for LIBs owing to its highest known capacity (4200 mAh g^{-1}), which is around ten times higher than that of graphite (372 mAh g^{-1}). However, the huge volume changes during Li-ion insertion ($>300\%$), low electronic conductivity, high capacity, fading, and pulverization over cycling hinder its pristine practical applications.^[308–315] The blending of silicon with various carbonaceous materials is one of the effective strategies to overcome the above-mentioned issues and improve its overall electrochemical performance.^[243,297,316–323] To illustrate, the boron-doped nano/microstructured silicon carbon nanotube composite with graphite framework (B–Si/CNT@G) developed by P–Li et al.^[324] exhibited excellent capacity retention of 84% after 100 cycles with an ultrahigh active mass loading of 11.2 mg cm^{-2} , which is outstripping the commercial active mass loading of graphite. Besides, the full cell LIBs fabricated with 2 mol% Al-doped full-concentration-gradient $\text{Li}[\text{Ni}_{0.76}\text{Co}_{0.09}\text{Mn}_{0.15}]\text{O}_2$ (Al2-FCG76) display a higher areal energy density of 8.0 mWh cm^{-2} even with a higher cathodic mass loading of 12.0 mg cm^{-2} and exhibit excellent capacitive retention (~82.5%) over 300 cycles (Figure 7a). X. Zhang et al.^[316] developed a design protocol for

two-dimensional covalent encapsulation of silicon to address the large volume change, low rate capability, and cycling stability of silicon by improving the contact between the silicon and electrically conductive media (Figure 7b). The SF@G hybrid electrode material, synthesized through the conformal deposition of graphene nanosheets (2~3 layers) on silicene flowers (SF) through the CVD process, exhibits a higher stability and rate capability, which is attributed to the covalent encapsulation of silicon, which blocks the direct electrolyte contact with the silicon and, also, enables fast electron and ion transport from and to the silicon, respectively. Similarly, other nanocarbons, such as Graphene Oxide, CNTs, CNFs, etc., were also explored to improve the electrochemical performance of silicon.^[243,325–335] The encapsulation of silicon nanowires with reduced graphene oxide (SiNW@G@RGO) by Wang et al.^[318] builds a self-supporting binder-free silicon-based anodes which exhibit a high reversible specific capacity of 1600 mAh g^{-1} (@ 2.1 A g^{-1}) with 80% capacity retention after 100 cycles and also maintain a very high Li-ion storage capacity of 500 mAh g^{-1} at a high current density of 8.4 A g^{-1} . Fu et al.^[336] fabricated a freestanding aligned Si–CNT sheet anode showing a very high specific capacity of 1494 mAh g^{-1} even after 45 cycles with a capacity retention of over 94% with a stabilized high coulombic efficiency of above 98%. It also retained a high specific capacity of 1000 mAh g^{-1} at a high current density of 800 mA/g . This improved electrochemical performance is attributed to the horizontal super-aligned CNT sheets, which provide high surface area as well as the porous structure that facilitates the Li-ions towards the silicon. The inclusion of silicon in CNFs resolves various issues, such as the pulverization process during prolonged cycling, improving the cycle life, vulnerable contacts between Si and carbon conductors, and unstable solid-electrolyte interphase. The core-shell Si–CNF structure fiber electrodes prepared by Hwang et al.^[337] by an electrospinning process using a dual nozzle in a scalable manner exhibit a gravimetric capacity as high as 1384 mAh g^{-1} and a high discharge capacity of 721 mAh g^{-1} within 5-minute discharge rate, also maintaining 300 cycles with high initial capacity retention. Similarly, a plethora of research activities are going around to improve the electrochemical performance of silicon material in cooperation with different carbon composites.^[338,339]

The carbon composites with metal oxides have gotten greater attention as not only anode materials but also cathode materials for LIBs.^[339–346] For example, M. Sathiya et al.^[347] developed a V_2O_5 -Anchored CNTs ($\text{V}_2\text{O}_5/\text{CNTs}$) nanocomposite as cathode material for LIBs, exhibiting a very high rate capability with a paramount non-diffusive Li-ion insertion storage, as elucidated from the power law method (Figure 7c). The enhanced capacity with high-power property achieved by $\text{V}_2\text{O}_5/\text{CNTs}$ is attributed to the unique structural property, which includes the short Li-ion diffusion pathway, easy accessibility to the vanadium centers, and high electronic conductivity offered by the CNTs structures. H. SUN et al.^[151] synthesized a 3D holey graphene/ Nb_2O_5 composite ($\text{Nb}_2\text{O}_5/\text{HGF}$) with tailored porosity architecture that is utilized as anode material for ultra-high-power Li-ion storage. The composite exhibits a specific and areal capacity at an exceptionally high power rate of 100 C ,

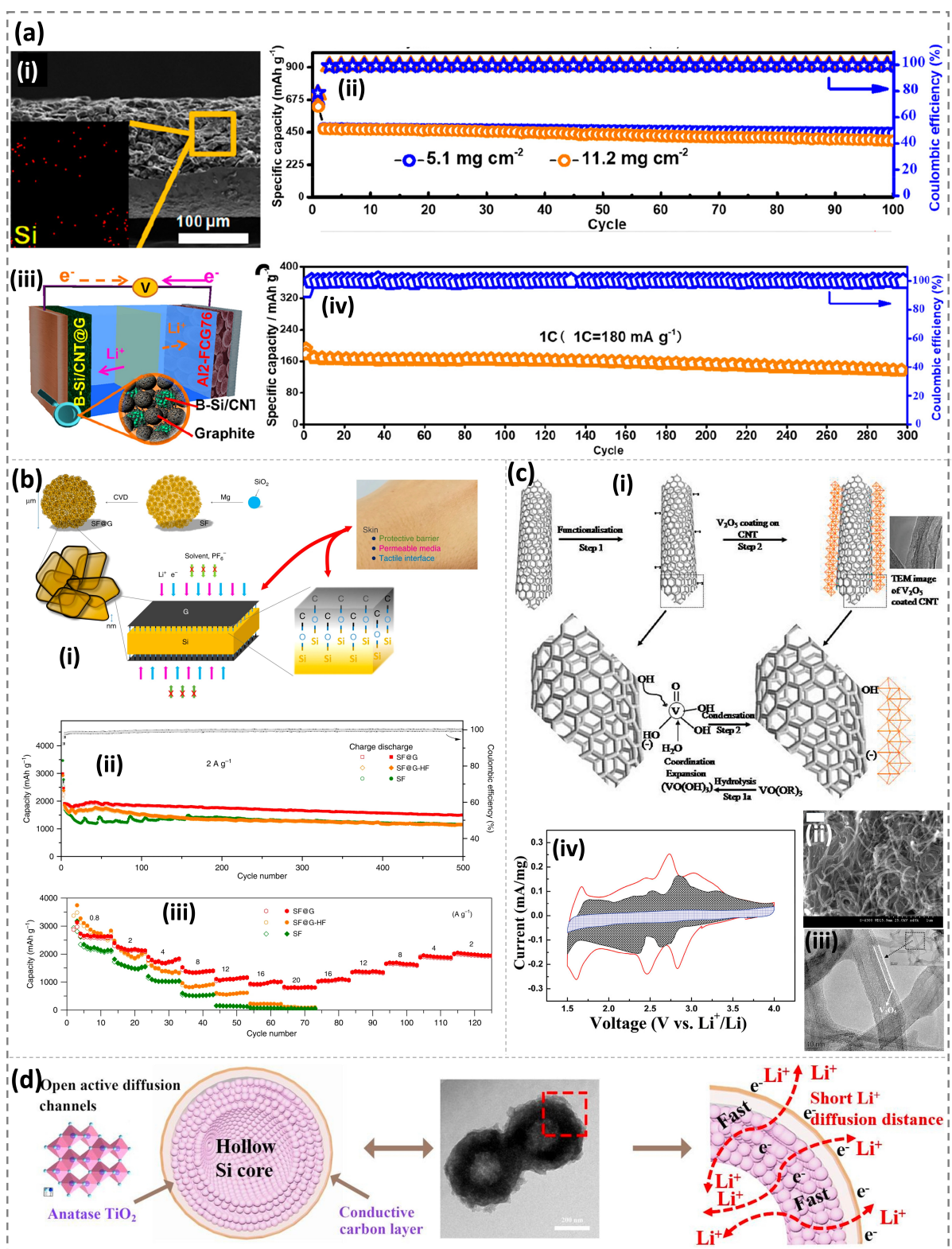


Figure 7. (a) (i) SEM images of B-Si/CNT@G electrode, and (ii) the half-cell cycling stability performance with different ultra-high loading against the Li-metal, (iii) schematic illustration of LIB with B-Si/CNT@G and Al2-FCG76 as anode and cathode, respectively, and their cycling performance at 1 C rate. Reproduced from ref.^[324] Copyright 2019, with permission from the American Chemical Society. (b) (i) Schematic illustration of the fabrication process for SF@G, the enhanced (ii) cycling stability, and (iii) rate capability shown by SF@G compared to other electrode configurations. Reproduced from ref.^[316] Copyright 2020, with permission from Springer Nature (c) (i) Schematic representation of the synthesis and structure of V₂O₅/CNTs, the (ii) SEM, and (iii) TEM images showing the morphology of the V₂O₅/CNTs. (iv) the cyclic voltammogram of V₂O₅/CNTs with Li-metal differentiating the capacitive (shaded grey area) and diffusion-controlled charge storage contributions. Reproduced from ref.^[347] Copyright 2011, with permission from the American Chemical Society. (c) Schematic representation of dual stabilized monodisperse hollow Si@TiO₂@C nanosphere showing Li-ion diffusion path. Reproduced from ref.^[349] Copyright 2018, with permission from the Elsevier.

indicating that the tailored porosity in the 3D conductive holey graphene scaffold facilitates the charge transport and shows high-rate Li-ion storage even at the commercial mass loading condition. Similarly, many other metal oxides improve the electrochemical performances in combination with carbon matrixes. For example, the embedding of Mn_3O_4 nanoparticles on reduced graphene oxide (RGO) sheets ($\text{Mn}_3\text{O}_4/\text{RGO}$) reported by Wang et al.^[299] by a two-step solution-phase reactions show a high specific capacity of up to $\sim 900 \text{ mAh g}^{-1}$, near the theoretical capacity of Mn_3O_4 , can be considered as a potential high-capacity, low-cost, and environmentally friendly anode candidate for LIBs. Another case of Co_3O_4 nanoparticles anchored on conducting graphene nanocomposites synthesized by Wu et al.^[348] shows the potential as an advanced anode material for high-performance LIBs. In $\text{Co}_3\text{O}_4/\text{graphene}$ composites, the Co_3O_4 nanoparticles having 10–30 nm in size are homogeneously anchored on graphene sheets, which also act as spacers to keep the neighboring graphene sheets separated. Additionally, the strong interaction between Co_3O_4 nanoparticles and graphene sheets prevents the volume expansion/contraction and aggregation of Co_3O_4 during the Li charge/discharge process. The $\text{Co}_3\text{O}_4/\text{graphene}$ composite exhibits a large specific capacity of $\sim 935 \text{ mAh g}^{-1}$ after 30 cycles and a better rate capability with a reversible capacity of 800 mAh g^{-1} (50 mA g^{-1}) with excellent cyclic stability and coulombic efficiency of above $\sim 98\%$.

The 3D carbon nanocomposites are another promising category showing enhanced electrochemical performances in terms of higher coulombic efficiencies and cycling stability. The alloy/conversion materials wrapped by carbon matrixes in a spherical hierarchical structure provide superior kinetic Li-ion transport and also mitigate the volume expansion. For instance, B. Lu et al.^[349] successfully crafted a dual-stabilized, monodisperse hollow $\text{Si@TiO}_2@\text{C}$ nanosphere. This hierarchical structure establishes a conductive and stable framework, shortening the Li-ion diffusion path, facilitating fast kinetics, and preventing the fracture and pulverization of the Si host during the Li insertion/de-insertion process. The synthesized material demonstrated an exceptionally high initial specific discharge capacity of $2557.1 \text{ mAh g}^{-1}$, achieving an ICE of 86.06% at 0.2 A g^{-1} . Furthermore, it exhibited admirable cycling stability, maintaining a specific capacity of $1270.3 \text{ mAh g}^{-1}$ after 250 cycles at 1 A g^{-1} , with a mean coulombic efficiency of 99.53% . Table 2 provides a comprehensive overview of the electrochemical performances of different carbon-nanostructure composites having 1D, 2D, and 3D carbon matrixes developed via different synthesis methods.

From the analysis of different carbon-based composites in various reports, it is evident that the carbon matrixes support the active materials by increasing the electronic and ionic conductivities, buffering the volume change, and providing better interfacial contact with the electrode in combination with the utilization of active Li-ion storage materials.

3. Conclusion and Outlook

This review covers a range of carbon-based materials, spanning from bulk to the nanoscale, employed for Li-ion storage applications. As shown, graphite is still the preferable commercial anode material for LIBs; however, more investigations should be required to resolve issues such as limited Li-insertion capacity and Li-plating at higher current rates, etc., to improve the LIB performance. Different strategies such as designing porous structures, incorporating alloy/conversion materials in graphite structures, etc., are adopted to improve the storage capacity as well as for high-power applications. Non-graphitizable hard carbon (HC) and graphitizable soft carbon (SC) are considered potential alternative anode materials to LIBs due to their higher specific capacity compared to graphite, which also depends upon their degree of structural disorder. Among these, HC displays higher Li-storage capacity due to its large disorder structure, in which Li-adsorption is also happening in addition to the intercalation, where the exact Li-insertion mechanism is still debatable. On the other hand, due to the high electronic conductivity offered by the turbostratic disordered structure, the SCs can be considered for high-power Li-storage applications. Moreover, both HCs and SCs exhibit less electrode expansion rate compared to graphite, which provides long cycling durability for these materials. As evident, the increase in structural disorder enhances specific capacity by introducing additional adsorption and pore-filling Li storage mechanisms beyond Li-ion intercalation. However, the ICE of both HC and SC are less compared to graphite due to high irreversible loss in the initial cycle, which is required to be addressed by investigating the electrode/electrode surface engineering, creating a thin, homogeneous, stable SEI layer either artificially or by tuning the electrolyte components. Even though the safety is better in SC and HC compared to graphite, the sloping potential profile and the tap density of the material are unsuitable for commercial applications. These aspects heavily depend on the material synthesis methods, reaction environment, and the source of precursors, which in turn are bound to the cost of production.

The use of 1D, 2D, and 3D nanocarbons such as CNTs/CNFs, graphene, and carbon nanospheres, respectively, opens a new vista of energy materials with highly electroactive surface areas, which improves electrolyte wettability as well as Li-storage capacity. Moreover, in the nano realm, the carbon materials showed anomalous behaviors in terms of improved electronic and ionic conductivities, reducing the Li-ion diffusion length and hence facilitating the diffusion, primarily advantageous for high-power applications. Since the Li-ion storage capacity of these materials relies on factors such as morphology, high surface area, and porosity, it is imperative to implement modifications and optimizations in the synthesis method, precursor selection, etc., for designing hierarchical nanostructures. Further, an appropriate blending of carbon matrices with diverse alloy/conversion materials creates complex nanocomposites that can exhibit improved electrochemical performances, addressing challenges like the pulverization effect stemming from substantial volume expansion and low electronic con-

Table 2. Electrochemical performance of different carbon nanocomposites.

Composites	Synthesis Method	Initial discharge capacity (mAh g ⁻¹)	Initial Coulombic Efficiency (ICE, %)	Cycling Stability (cycles)	Ref
<i>1D Carbon nanostructures composites</i>					
Vertically aligned multiwall CNTs (VACNTs)/silicon nanocomposites	CVD	2552 (@100 mAg ⁻¹)	80.3	100 (1000 mAh g ⁻¹ @C/10)	[350]
Free-Standing CNT–Si Films	CVD	2083 (@ C/10)	86	50 (1711 mAh g ⁻¹ @C/10)	[351]
Sn nanoparticles @CNT	Chemical reduction	1114 (@30 mAg ⁻¹)	56.6	100 (413 mAh g ⁻¹)	[352]
Nano-SnO ₂ /CNT hairball	Solvothermal	2255 (@100 mAg ⁻¹)	48.7	100 (809.2 mAh g ⁻¹ @200 mAg ⁻¹)	[353]
Co ₃ O ₄ nanoparticle @CNT	Ultrasonication	1045 (@200 mAg ⁻¹)	71.8	70 (940 mAh g ⁻¹ @200 mAg ⁻¹)	[354]
CNF/Mn ₃ O ₄ coaxial nanocables	electrospinning and Electrophoretic deposition	1690 (@100 mAg ⁻¹)	55.4	50 (760 mAh g ⁻¹ @100 mAg ⁻¹)	[355]
Multi-Wall Sn/SnO ₂ @Carbon Hollow Nanofiber	Electrospinning	1961 (@1000 mAg ⁻¹)	57.2	2000 (986 mAh g ⁻¹ @1000 mAg ⁻¹)	[356]
Porous Sn/CoSn _x @C nanotubes	Electrospun	2006.6 (@1000 mAg ⁻¹)	55.25	10000 (265.5 mAh g ⁻¹ @8000 mAg ⁻¹)	[357]
<i>2D Carbon nanostructures composites</i>					
SnO ₂ /Co ₃ O ₄ /rGO composite	Hydrothermal	1787 (@50 mAg ⁻¹)	63.4	100 (727 mAh g ⁻¹ @100 mAg ⁻¹)	[358]
MOF/SnO ₂ /Graphene	Wet Impregnation	1086 (@1000 mAg ⁻¹)	47	1000 (450 mAh g ⁻¹ @1000 mAg ⁻¹)	[359]
SiNW@G@RGO	CVD and filtration	~2000 (@210 mAg ⁻¹)	~50	100 (1600 mAh g ⁻¹ @2100 mAg ⁻¹)	[318]
Mn ₃ O ₄ /graphene nanocomposite	Single-step hydrothermal	~1400 (@20 mAg ⁻¹)	~50	200 (~474 mAh g ⁻¹ @100 mAg ⁻¹)	[199]
γ-MnOOH-rGO nanocomposite	Hydrothermal	~1515 (@100 mAg ⁻¹)	41%	500 (~528 mAh g ⁻¹ @100 mAg ⁻¹)	[200]
TiNb ₂ O ₇ /Graphene	Solvothermal	~303 (@C/10)	~83	300 (~200 mAh g ⁻¹ @1 C)	[198]
<i>3D Carbon nanostructure composites</i>					
SnO ₂ –CNT composite microspheres	spray pyrolysis	1459 (@1500 mAg ⁻¹)	73	1000 (796 mAh g ⁻¹ @4000 mAg ⁻¹)	[360]
B–Si/CNT@G	SPEX mill	2694 (@400 mAg ⁻¹)	80.2	200 (1415 mAh g ⁻¹ @2000 mAg ⁻¹)	[324]

Table 2. continued

Composites	Synthesis Method	Initial discharge capacity (mAh g ⁻¹)	Initial Coulombic Efficiency (ICE, %)	Cycling Stability (cycles)	Ref
Nanosized yolk-shell-structured (YSS) Co ₃ O ₄ @C	Carbonization through heat treatment	1190 (@100 mAh g ⁻¹)	75.7	300 (626 mAh g ⁻¹ @1000 mAh g ⁻¹)	[361]
Zeolitic imidazolate framework-8 (ZIF-8) derived carbon (Mn ₂ SiO ₄ @C)	Hydrothermal	1825 (@200 mAh g ⁻¹)	59	500 (554 mAh g ⁻¹ @5000 mAh g ⁻¹)	[362]
Hollow Si@TiO ₂ @C nanosphere	Magnesiothermic Reduction, Sol-Gel	2557 (@200 mAh g ⁻¹)	86	400 (1058 mAh g ⁻¹ @ 4000 mAh g ⁻¹)	[349]
Mesoporous C@SnO ₂ @C hollow nanospheres	Stober's, Hydrothermal	1484 (@200 mAh g ⁻¹)	57.5	10000 (400 mAh g ⁻¹ @5000 mAh g ⁻¹)	[363]

ductivity, commonly observed in alloy/conversion materials. Additionally, the use of nanocarbon provides an electronic and ionic conductive path, which can enhance the Li-ion diffusion, efficiency, and stability of the metal oxides not only for anode materials but also for the cathode materials. More interestingly, nanocarbons play a vital role in developing flexible electrodes, which is imperative for the development of wearable technologies. Despite the tremendous advantages, the nanocarbons are hindered by the excessive irreversible initial charge storage due to the highly defective surfaces, which consume a lot of electrolytes. These can be tackled through the development of novel hierachal carbon structures that can offer highly reversible redox reactions or by impregnating carbon nanostructures with pre-lithiation, which can compensate for the loss of Li-inventory during the working of full-cell LIBs. It is worth notifying that nanocarbon production for LIBs is still in an immature stage, requiring new protocols to scale up nanocarbons to the commercial level without escalating the cost of production.

In the quest for anode materials, numerous bulk and nanomaterials stand as alternative candidates to conventional graphite. Nevertheless, significant research efforts are required to develop mature technologies that can elevate them to commercial viability. Despite the high specific capacity, the main common challenge faced by these alternative materials is the low ICE. To tackle this problem, it is essential to understand the basic reason, which depends upon the types of anode materials.^[74] For instance, the low ICE in intercalation materials is due to the irreversible adsorption of Li-ions apart from the SEI layer. In the case of alloy/conversion materials, factors such as the irreversible decomposition of oxides and sulfides, along with irreversible reactions stemming from the coarsening of active materials, collectively contribute to the low ICE in addition to the SEI layer formation and irreversible adsorption of Li-ions. Numerous compelling approaches, such as minimizing side reactions, controlling the formation of the SEI layer, facilitating the reversible decomposition of oxides and sulfides, and inhibiting the coarsening of nanomaterials, must be employed to mitigate the initial coulombic loss. In spite of the

improved ICE exhibited by some hierachal carbon nanostructures,^[364,365] the challenge of low ionic conductivity is not completely addressed by solely developing carbon composite structures. This is because the carbon matrices themselves experience irreversible charge loss attributed to the formation of a thick SEI layer. Pre-lithiation is one of the techniques used to overcome the overconsumption of Li-ion by the SEI layer. In-situ pre-lithiation is the more viable and cost-effective method, which can be implemented through the electrolyte additive or by mixing sacrificial agents with the cathode materials during LIB fabrication.^[366,367] Different electrolyte additives such as fluoroethylene carbonate, LiF, vinyl carbonate, dioxolone derivatives, etc.,^[368-370] contribute to the formation of a stable and uniform solid electrolyte interface (SEI) layer. This mitigates excessive electrolyte consumption and prevents potential dendrite formation, thereby enhancing the ICE and ensuring prolonged cycling stability. Additionally, the incorporation of organic or inorganic salts as sacrificial agents with cathode active materials compensates for irreversible capacity loss in the initial cycle, further improving overall cycling stability.^[366,371] Innovative electrolyte designs, including combinations of ether and ionic liquids, as well as solvated ionic liquids, could be promising alternatives that can enhance the efficiency of lithium-ion batteries (LIBs) when compared to conventional ester-based carbonate organic electrolytes.^[372-375] Another prevalent challenge involves the low tap density and substantial material synthesis costs in comparison to graphite, a critical factor in evaluating commercial viability. This issue is predominantly influenced by factors such as precursor sources, synthesis methods, reaction environments, etc.

In summary, achieving the effective utilization of alternative carbon-based materials at the commercial scale requires a more precise understanding of the lithium-storage mechanisms in various carbon compounds. This necessitates comprehensive evaluation through diverse in-situ and operando analyses, enabling the engineering of materials for enhanced reversibility in electrochemical reactions. To achieve this goal, the development of new technologies and strategies is imperative, leveraging the strengths of theoretical and simulated ap-

proaches to design novel carbon materials featuring hierarchical and robust structures in a cost-effective manner. Additionally, elucidating the components of the SEI layer is crucial to establishing a thin, homogeneous, ion-conductive, flexible, self-healing, and stable SEI layer, ultimately enhancing the initial coulombic efficiency. Thus, to propel the LIBs towards meeting high power and energy requirements with increased stability, simultaneous evaluation of both electrode materials and electrolytes is essential.

Acknowledgements

The author would like to acknowledge Shiv Nadar Institution of Eminence, India for providing necessary academic resources during manuscript preparation.

Conflict of Interests

The authors declare that they have no known competing financial interests or personal relationships that could have appeared to influence the work reported in this paper.

Keywords: Carbon Nanofibers · Carbon Nanotubes · Graphene · Graphite · Hard carbon · Soft carbon · Nanocarbon

- [1] B. Diouf, R. Pode, *Renewable Energy* **2015**, *76*, 375.
- [2] J. B. Goodenough, K.-S. Park, *J. Am. Chem. Soc.* **2013**, *135*, 1167.
- [3] J. B. Goodenough, *Acc. Chem. Res.* **2013**, *46*, 1053.
- [4] J. B. Goodenough, *ACS Catal.* **2017**, *7*, 1132.
- [5] P. G. Bruce, *Solid State Ionics* **2008**, *179*, 752.
- [6] P. U. Nzereogu, A. D. Omah, F. I. Ezema, E. I. Iwuoha, A. C. Nwanya, *Applied Surface Science Advances* **2022**, *9*, 100233.
- [7] H. Azuma, H. Imoto, S. Yamada, K. Sekai, *J. Power Sources* **1999**, *81*(82), 1.
- [8] N. Takami, *J. Electrochem. Soc.* **1995**, *142*, 371.
- [9] J. Lach, K. Wróbel, J. Wróbel, A. Czerwiński, *Energies* **2021**, *14* (9), 2649.
- [10] N. A. Kaskhedikar, J. Maier, *Adv. Mater.* **2009**, *21*, 2664.
- [11] Y. Jiang, J. Jiang, P. Nie, W. Guo, C. Geng, Z. Sun, Y. Fei, Y. Chen, Q. Zhuang, Z. Xing, Z. Ju, H. Shao, *J. Energy Storage* **2023**, *72*, 108484.
- [12] Y. Nishi, *Chem. Rec.* **2001**, *1*, 406.
- [13] B. N. Loeffler, D. Bresser, S. Passerini, M. Copley, Johnson Matthey, *Technol. Rev.* **2**(59), 34.
- [14] K. Mizushima, P. C. Jones, P. J. Wiseman, J. B. Goodenough, *Mater. Res. Bull.* **1980**, *15*, 783.
- [15] M. Winter, B. Barnett, K. Xu, *Chem. Rev.* **2018**, *118*, 11433.
- [16] A. Satoh, N. Takami, T. Ohsaki, *Solid State Ionics* **1995**, *80*, 291.
- [17] S. J. An, J. Li, C. Daniel, D. Mohanty, S. Nagpure, D. L. Wood, *Carbon* **2016**, *105*, 52.
- [18] J. B. Goodenough, Y. Kim, *Chem. Mater.* **2010**, *22*, 587.
- [19] J. B. Goodenough, Y. Kim, *J. Power Sources* **2011**, *196*, 6688.
- [20] R. D. Deshpande, D. M. Bernardi, *J. Electrochem. Soc.* **2017**, *164*, A461.
- [21] A. Wang, S. Kadam, H. Li, S. Shi, Y. Qi, *npj Computational Materials* **2018**, *4*, 15.
- [22] R. Okuno, M. Yamamoto, A. Kato, M. Takahashi, *Electrochim. Commun.* **2022**, *138*, 107288.
- [23] Y. Cai, C. Fan, *Electrochim. Acta* **2011**, *58*, 481.
- [24] S. Kuroda, N. Tobori, M. Sakuraba, Y. Sato, *J. Power Sources* **2003**, *119*(121), 924.
- [25] Y. Sun, X.-L. Shi, Y.-L. Yang, G. Suo, L. Zhang, S. Lu, Z.-G. Chen, *Adv. Funct. Mater.* **2022**, *32*, 2201584.
- [26] C. Hernández-Rentero, V. Marangon, M. Olivares-Marín, V. Gómez-Serrano, Á. Caballero, J. Morales, J. Hassoun, *J. Colloid Interface Sci.* **2020**, *573*, 396.
- [27] K. Yu, J. Li, H. Qi, C. Liang, *Diamond Relat. Mater.* **2018**, *86*, 139.
- [28] P. Molaiyan, G. S. Dos Reis, D. Karuppiah, C. M. Subramaniyam, F. García-Alvarado, U. Lassi, *Batteries* **2023**, *9* (2), 116.
- [29] R. A. Adams, A. Varma, V. G. Pol, *Adv. Energy Mater.* **2019**, *9*, 1900550.
- [30] M. Winter, J. O. Besenhard, M. E. Spahr, P. Novák, *Adv. Mater.* **1998**, *10*, 725.
- [31] B. Babu, P. Simon, A. Balducci, *Adv. Energy Mater.* **2020**, *10*, 2001128.
- [32] L. Xie, C. Tang, Z. Bi, M. Song, Y. Fan, C. Yan, X. Li, F. Su, Q. Zhang, C. Chen, *Adv. Energy Mater.* **2021**, *11*, 2101650.
- [33] L.-F. Zhao, Z. Hu, W.-H. Lai, Y. Tao, J. Peng, Z.-C. Miao, Y.-X. Wang, S.-L. Chou, H.-K. Liu, S.-X. Dou, *Adv. Energy Mater.* **2021**, *11*, 2002704.
- [34] J. J. H. Togonon, P.-C. Chiang, H.-J. Lin, W.-C. Tsai, H.-J. Yen, *Carbon Trends* **2021**, *3*, 100035.
- [35] W. Rüdorff, U. Hofmann, Z. Anorg. Allg. Chem. **1938**, *238*, 1.
- [36] J. O. Besenhard, *Carbon* **1976**, *14*, 111.
- [37] D. Bar-Tov, E. Peled, L. Burstein, *J. Electrochem. Soc.* **1999**, *146*, 824.
- [38] D. Allart, M. Montaru, H. Gualous, *J. Electrochem. Soc.* **2018**, *165*, A380.
- [39] M. Yoshio, H. Wang, K. Fukuda, T. Umeno, T. Abe, Z. Ogumi, *J. Mater. Chem.* **2004**, *14*, 1754.
- [40] M. Simón, A. Benítez, A. Caballero, J. Morales, O. Vargas, *Batteries* **2018**, *4* (1), 13.
- [41] R. C. Boehm, A. Banerjee, *J. Chem. Phys.* **1992**, *96*, 1150.
- [42] J. B. Siegel, A. G. Stefanopoulou, P. Hagans, Y. Ding, D. Gorsich, *J. Electrochem. Soc.* **2013**, *160*, A1031.
- [43] S. Schweidler, L. de Biasi, A. Schiele, P. Hartmann, T. Brezesinski, J. Janek, *J. Phys. Chem. C* **2018**, *122*, 8829.
- [44] H. Michael, F. Iacoviello, T. M. M. Heenan, A. Llewellyn, J. S. Weaving, R. Jervis, D. J. L. Brett, P. R. Shearing, *J. Electrochem. Soc.* **2021**, *168*, 010507.
- [45] T. Tran, K. Kinoshita, *J. Electroanal. Chem.* **1995**, *386*, 221.
- [46] K. Persson, V. A. Sethuraman, L. J. Hardwick, Y. Hinuma, Y. S. Meng, A. van der Ven, V. Srinivasan, R. Kostecki, G. Ceder, *J. Phys. Chem. Lett.* **2010**, *1*, 1176.
- [47] D. Billaud, F. X. Henry, M. Lelaurain, P. Willmann, *J. Phys. Chem. Solids* **1996**, *57*, 775.
- [48] J. Xu, Y. Dou, Z. Wei, J. Ma, Y. Deng, Y. Li, H. Liu, S. Dou, *Adv. Sci.* **2017**, *4*, 1700146.
- [49] V. A. Sethuraman, L. J. Hardwick, V. Srinivasan, R. Kostecki, *J. Power Sources* **2010**, *195*, 3655.
- [50] A. Funabiki, M. Inaba, T. Abe, Z. Ogumi, *J. Electrochem. Soc.* **2019**, *146*, 2443.
- [51] K. Persson, Y. Hinuma, Y. S. Meng, A. Van der Ven, G. Ceder, *Phys. Rev. B* **2010**, *82*, 125416.
- [52] W. Zhou, P. H.-L. Sit, *ACS Omega* **2020**, *5*, 18289.
- [53] H. Zhang, Y. Yang, D. Ren, L. Wang, X. He, *Energy Storage Mater.* **2021**, *36*, 147.
- [54] C. Wang, I. Kakwan, A. J. Appleby, F. E. Little, *J. Electroanal. Chem.* **2000**, *489*, 55.
- [55] M. Inaba, *J. Electrochem. Soc.* **1995**, *142*, 20.
- [56] M. D. Levi, E. Levi, Y. Gofer, D. Aurbach, E. Vieil, J. Serose, *J. Phys. Chem. B* **1999**, *103*, 1499.
- [57] C. Sole, N. E. Drewett, L. J. Hardwick, *Faraday Discuss.* **2014**, *172*, 223.
- [58] J. Zou, C. Sole, N. E. Drewett, M. Velický, L. J. Hardwick, *J. Phys. Chem. Lett.* **2016**, *7*, 4291.
- [59] C. Uhlmann, J. Illig, M. Ender, R. Schuster, E. Ivers-Tiffé, *J. Power Sources* **2015**, *279*, 428.
- [60] P. Maire, A. Evans, H. Kaiser, W. Scheifele, P. Novák, *J. Electrochem. Soc.* **2008**, *155*, A862.
- [61] Y. Chen, K.-H. Chen, A. J. Sanchez, E. Kazyak, V. Goel, Y. Gorlin, J. Christensen, K. Thornton, N. P. Dasgupta, *J. Mater. Chem. A* **2021**, *9*, 23522.
- [62] T. Gao, Y. Han, D. Fragedakis, S. Das, T. Zhou, C.-N. Yeh, S. Xu, W. C. Chueh, J. Li, M. Z. Bazant, *Joule* **2021**, *5*, 393.
- [63] H. Wang, Y. Zhu, S. C. Kim, A. Pei, Y. Li, D. T. Boyle, H. Wang, Z. Zhang, Y. Ye, W. Huang, Y. Liu, J. Xu, J. Li, F. Liu, Y. Cui, *Proc. Natl. Acad. Sci. USA* **2020**, *117*, 29453.
- [64] G. Yang, X. Li, Z. Guan, Y. Tong, B. Xu, X. Wang, Z. Wang, L. Chen, *Nano Lett.* **2020**, *20*, 3836.
- [65] M. A. Cabañero, M. Hagen, E. Quiroga-González, *Electrochim. Acta* **2021**, *374*, 137487.
- [66] V. A. Nalimova, D. Guérard, M. Lelaurain, O. V. Fateev, *Carbon* **1995**, *33*, 177.
- [67] J. Asenbauer, T. Eisenmann, M. Kuenzel, A. Kazzazi, Z. Chen, D. Bresser, *Sustain. Energy Fuels* **2020**, *4*, 5387.
- [68] E. P. M. Leiva, *J. Solid State Electrochem.* **2020**, *24*, 2117.

- [69] N. Sharma, W. K. Pang, Z. Guo, V. K. Peterson, *ChemSusChem* **2015**, *8*, 2826.
- [70] N. Li, D. Su, *Carbon Energy* **2019**, *1*, 200.
- [71] Z. Guo, X. Tian, Y. Song, T. Yang, Z. Ma, X. Gong, C. Wang, *Coating* **2023**, *13*.
- [72] Z. Guo, Z. Xu, F. Xie, J. Jiang, K. Zheng, S. Alabidun, M. Crespo-Ribadeneyra, Y.-S. Hu, H. Au, M.-M. Titirici, *Adv. Mater.* **2023**, *2304091*.
- [73] J. Xiao, Q. Li, Y. Bi, M. Cai, B. Dunn, T. Glossmann, J. Liu, T. Osaka, R. Sugiura, B. Wu, J. Yang, J.-G. Zhang, M. S. Whittingham, *Nat. Energy* **2020**, *5*, 561.
- [74] X. Li, X. Sun, X. Hu, F. Fan, S. Cai, C. Zheng, G. D. Stucky, *Nano Energy* **2020**, *77*, 105143.
- [75] W. Xing, J. R. Dahn, *J. Electrochem. Soc.* **1997**, *144*, 1195.
- [76] M. Drews, J. Büttner, M. Bauer, J. Ahmed, R. Sahu, C. Scheu, S. Vierrath, A. Fischer, D. Biro, *ChemElectroChem* **2021**, *8*, 4750.
- [77] E. Buiel, J. R. Dahn, *Electrochim. Acta* **1999**, *45*, 121.
- [78] Y. Abe, T. Saito, S. Kumagai, *Batteries* **2018**, *4* (4), 71.
- [79] K. Zou, W. Deng, P. Cai, X. Deng, B. Wang, C. Liu, J. Li, H. Hou, G. Zou, X. Ji, *Adv. Funct. Mater.* **2021**, *31*, 2005581.
- [80] X. Zhang, H. Qu, W. Ji, D. Zheng, T. Ding, C. Abegglen, D. Qiu, D. Qu, *ACS Appl. Mater. Interfaces* **2020**, *12*, 11589.
- [81] N. Ren, L. Wang, X. He, L. Zhang, J. Dong, F. Chen, J. Xiao, B. Pan, C. Chen, *ACS Appl. Mater. Interfaces* **2021**, *13*, 46813.
- [82] D. Saurel, J. Segalini, M. Jauregui, A. Pendashteh, B. Daffos, P. Simon, M. Casas-Cabanás, *Energy Storage Mater.* **2019**, *21*, 162.
- [83] E. Irisarri, N. Amini, S. Tennison, C. M. Ghimbeu, J. Gorka, C. Vix-Guterl, A. Ponrouch, M. R. Palacin, *J. Electrochem. Soc.* **2018**, *165*, A4058.
- [84] S. Alvin, H. S. Cahyadi, J. Hwang, W. Chang, S. K. Kwak, J. Kim, *Adv. Energy Mater.* **2020**, *10*, 2000283.
- [85] D. A. Stevens, J. R. Dahn, *J. Electrochem. Soc.* **2001**, *148*, A803.
- [86] Y. Huang, Y. Wang, P. Bai, Y. Xu, *ACS Appl. Mater. Interfaces* **2021**, *13*, 38441.
- [87] L. Zhang, W. (Alex) Wang, S. Lu, Y. Xiang, *Adv. Energy Mater.* **2021**, *11*, 2003640.
- [88] S. Huang, Z. Li, B. Wang, J. Zhang, Z. Peng, R. Qi, J. Wang, Y. Zhao, *Adv. Funct. Mater.* **2018**, *28*, 1706294.
- [89] C.-W. Tai, W.-Y. Jao, L.-C. Tseng, P.-C. Wang, A.-P. Tu, C.-C. Hu, *J. Mater. Chem. A* **2023**, *11*, 19669.
- [90] J. Yang, X. Zhou, J. Li, Y. Zou, J. Tang, *Mater. Chem. Phys.* **2012**, *135*, 445.
- [91] W. Li, M. Chen, C. Wang, *Mater. Lett.* **2011**, *65*, 3368.
- [92] J. Ni, Y. Huang, L. Gao, *J. Power Sources* **2013**, *223*, 306.
- [93] A. Piotrowska, K. Kierzek, P. Rutkowski, J. Machnikowski, *J. Anal. Appl. Pyrolysis* **2013**, *102*, 1.
- [94] T. Zheng, Q. Zhong, J. R. Dahn, *J. Electrochem. Soc.* **1995**, *142*, L211.
- [95] C. Wan Park, S.-H. Yoon, S. I. Lee, S. M. Oh, *Carbon* **2000**, *38*, 995.
- [96] F. Xie, Z. Xu, Z. Guo, M.-M. Titirici, *Progress in Energy* **2020**, *2*, 042002.
- [97] X. Dou, I. Hasa, M. Hekmatfar, T. Diemant, R. J. Behm, D. Buchholz, S. Passerini, *ChemSusChem* **2017**, *10*, 2668.
- [98] X. Lin, Y. Liu, H. Tan, B. Zhang, *Carbon* **2020**, *157*, 316.
- [99] L.-J. Xie, C. Tang, M.-X. Song, X.-Q. Guo, X.-M. Li, J.-X. Li, C. Yan, Q.-Q. Kong, G.-H. Sun, Q. Zhang, F.-Y. Su, C.-M. Chen, *J. Energy Chem.* **2022**, *72*, 554.
- [100] S. Ghosh, R. Santhosh, S. Jeniffer, V. Raghavan, G. Jacob, K. Nanaji, P. Kolla, S. K. Jeong, A. N. Grace, *Sci. Rep.* **2019**, *9*, 16315.
- [101] L. Li, C. Fan, B. Zeng, M. Tan, *Mater. Chem. Phys.* **2020**, *242*, 122380.
- [102] C. Ge, Z. Fan, J. Zhang, Y. Qiao, J. Wang, L. Ling, *RSC Adv.* **2018**, *8*, 34682.
- [103] R. S. Patil, A. Khandelwal, K. Y. Kim, K. S. Hariharan, S. M. Kolake, *J. Electrochem. Soc.* **2019**, *166*, A1185.
- [104] K.-H. Chen, V. Goel, M. J. Namkoong, M. Wied, S. Müller, V. Wood, J. Sakamoto, K. Thornton, N. P. Dasgupta, *Adv. Energy Mater.* **2021**, *11*, 2003336.
- [105] T. D. Tran, D. J. Derwin, P. Zaleski, X. Song, K. Kinoshita, *J. Power Sources* **1999**, *81*(82), 296.
- [106] I. Mochida, Y. Korai, C.-H. Ku, F. Watanabe, Y. Sakai, *Carbon* **2000**, *38*, 305.
- [107] C. Del Río, M. C. Ojeda, J. L. Acosta, *J. Appl. Polym. Sci.* **1999**, *74*, 1003.
- [108] W. Jiang, T. Tran, X. Song, K. Kinoshita, *J. Power Sources* **2000**, *85*, 261.
- [109] R. Alcántara, J. M. Jiménez Mateos, J. L. Tirado, *J. Electrochem. Soc.* **2002**, *149*, A201.
- [110] M. Wang, Y. Zhu, Y. Zhang, J. Duan, K. Wang, R. Wang, G. Sun, C. Wang, *J. Power Sources* **2021**, *481*, 228902.
- [111] L. Yan, Q. Ren, J. Wang, L. Fan, X. Mei, W. Lei, Z. Shi, *ACS Appl. Mater. Interfaces* **2022**, *14*, 48715.
- [112] A. Pendashteh, B. Orayech, H. Suhard, M. Jauregui, J. Ajuria, B. Silván, S. Clarke, F. Bonilla, D. Saurel, *Energy Storage Mater.* **2022**, *46*, 417.
- [113] A. Pendashteh, B. Orayech, J. Ajuria, M. Jáuregui, D. Saurel, *Energies* **2020**, *13*.
- [114] J. R. Dahn, A. K. Sleigh, H. Shi, J. N. Reimers, Q. Zhong, B. M. Way, *Electrochim. Acta* **1993**, *38*, 1179.
- [115] J. R. Dahn, T. Zheng, Y. Liu, J. S. Xue, *Science* **1995**, *270*, 590.
- [116] R. Fong, U. von Sacken, J. R. Dahn, *J. Electrochem. Soc.* **1990**, *137*, 2009.
- [117] M. Schroeder, S. Menne, J. Segalini, D. Saurel, M. Casas-Cabanás, S. Passerini, M. Winter, A. Balducci, *J. Power Sources* **2014**, *266*, 250.
- [118] M. Schroeder, M. Winter, S. Passerini, A. Balducci, *J. Electrochem. Soc.* **2012**, *159*, A1240.
- [119] M. Schroeder, M. Winter, S. Passerini, A. Balducci, *J. Power Sources* **2013**, *238*, 388.
- [120] Y.-N. Jo, M.-S. Park, E.-Y. Lee, J.-G. Kim, K.-J. Hong, S.-I. Lee, H. Y. Jeong, G. H. Ryu, Z. Lee, Y.-J. Kim, *Electrochim. Acta* **2014**, *146*, 630.
- [121] I. Mochida, C.-H. Ku, S.-H. Yoon, Y. Korai, *J. Power Sources* **1998**, *75*, 214.
- [122] R. Febrian, N. L. W. Septiani, M. Iqbal, B. Yuliarto, *J. Electrochem. Soc.* **2021**, *168*, 110520.
- [123] K. S. Novoselov, A. K. Geim, S. V. Morozov, D. Jiang, Y. Zhang, S. V. Dubonos, I. V. Grigorieva, A. A. Firsov, *Science* **2004**, *306*, 666.
- [124] R. Raccichini, A. Varzi, D. Wei, S. Passerini, *Adv. Mater.* **2017**, *29*, 1603421.
- [125] S. Goriparti, E. Miele, F. De Angelis, E. Di Fabrizio, R. Proietti Zaccaria, C. Capiglia, *J. Power Sources* **2014**, *257*, 421.
- [126] E. Yoo, J. Kim, E. Hosono, H. Zhou, T. Kudo, I. Honma, *Nano Lett.* **2008**, *8*, 2277.
- [127] C. Uthaisar, V. Barone, *Nano Lett.* **2010**, *10*, 2838.
- [128] E. Pollak, B. Geng, K.-J. Jeon, I. T. Lucas, T. J. Richardson, F. Wang, R. Kostecki, *Nano Lett.* **2010**, *10*, 3386.
- [129] E. Lee, K. A. Persson, *Nano Lett.* **2012**, *12*, 4624.
- [130] M. Kühne, F. Paolucci, J. Popovic, P. M. Ostrovsky, J. Maier, J. H. Smet, *Nat. Nanotechnol.* **2017**, *12*, 895.
- [131] P. Yu, B. N. Popov, J. A. Ritter, R. E. White, *J. Electrochem. Soc.* **1999**, *146*, 8.
- [132] J. H. Park, H. Yoon, Y. Cho, C.-Y. Yoo, *Materials* **2021**, *14*.
- [133] M. Kühne, F. Börrnert, S. Fecher, M. Ghorbani-Asl, J. Biskupek, D. Samuelis, A. V. Krasheninnikov, U. Kaiser, J. H. Smet, *Nature* **2018**, *564*, 234.
- [134] K. Ji, J. Han, A. Hirata, T. Fujita, Y. Shen, S. Ning, P. Liu, H. Kashani, Y. Tian, Y. Ito, J. Fujita, Y. Oyama, *Nat. Commun.* **2019**, *10*, 275.
- [135] D. W. Kim, S. M. Jung, C. Senthil, S.-S. Kim, B.-K. Ju, H. Y. Jung, *ACS Nano* **2021**, *15*, 797.
- [136] O. A. Vargas, C. Á. Caballero, J. Morales, *Nanoscale* **2012**, *4*, 2083.
- [137] P. Lian, X. Zhu, S. Liang, Z. Li, W. Yang, H. Wang, *Electrochim. Acta* **2010**, *55*, 3909.
- [138] H. F. Xiang, Z. D. Li, K. Xie, J. Z. Jiang, J. J. Chen, P. C. Lian, J. S. Wu, Y. Yu, H. H. Wang, *RSC Adv.* **2012**, *2*, 6792.
- [139] Z.-L. Wang, D. Xu, H.-G. Wang, Z. Wu, X.-B. Zhang, *ACS Nano* **2013**, *7*, 2422.
- [140] J. Tang, G. Chen, J. Yang, X. Zhou, L. Zhou, B. Huang, *Nano Energy* **2014**, *8*, 62.
- [141] H. Li, C. Lu, *Funct. Mater. Lett.* **2013**, *06*, 1350063.
- [142] B. Xing, H. Zeng, G. Huang, C. Zhang, R. Yuan, Y. Cao, Z. Chen, J. Yu, *J. Alloys Compd.* **2019**, *779*, 202.
- [143] H. Huang, H. Shi, P. Das, J. Qin, Y. Li, X. Wang, F. Su, P. Wen, S. Li, P. Lu, F. Liu, Y. Li, Y. Zhang, Y. Wang, Z.-S. Wu, H.-M. Cheng, *Adv. Funct. Mater.* **2020**, *30*, 1909035.
- [144] J. Yang, R. U. R. Sagar, T. Anwar, X. Li, Z. Qian, T. Liang, *Int. J. Energy Res.* **2022**, *46*, 5226.
- [145] Z. Fan, J. Yan, G. Ning, T. Wei, L. Zhi, F. Wei, *Carbon* **2013**, *60*, 558.
- [146] Y. Fang, Y. Lv, R. Che, H. Wu, X. Zhang, D. Gu, G. Zheng, D. Zhao, *J. Am. Chem. Soc.* **2013**, *135*, 1524.
- [147] K.-W. Kim, J. Kim, C. Choi, H. K. Yoon, M. C. Go, J. Lee, J. K. Kim, H. Seok, T. Kim, K. Wu, S. H. Kim, Y. M. Kim, J. H. Kwon, H. C. Moon, *ACS Appl. Mater. Interfaces* **2022**, *14*, 46994.
- [148] G. Ning, Y. Cao, C. Qi, X. Ma, X. Zhu, *J. Mater. Chem. A* **2017**, *5*, 9299.
- [149] D. Zhao, L. Wang, P. Yu, L. Zhao, C. Tian, W. Zhou, L. Zhang, H. Fu, *Nano Res.* **2015**, *8*, 2998.
- [150] Z. Zheng, X. Zhang, F. Pei, Y. Dai, X. Fang, T. Wang, N. Zheng, *J. Mater. Chem. A* **2015**, *3*, 19800.
- [151] H. Sun, L. Mei, J. Liang, Z. Zhao, C. Lee, H. Fei, M. Ding, J. Lau, M. Li, C. Wang, X. Xu, G. Hao, B. Papandrea, I. Shakir, B. Dunn, Y. Huang, X. Duan, *Science* **2017**, *356*, 599.

- [152] J. Zhang, B. Guo, Y. Yang, W. Shen, Y. Wang, X. Zhou, H. Wu, S. Guo, *Carbon* **2015**, *84*, 469.
- [153] Z. Du, W. Ai, C. Sun, C. Zou, J. Zhao, Y. Chen, X. Dong, J. Liu, G. Sun, T. Yu, W. Huang, *ACS Appl. Mater. Interfaces* **2016**, *8*, 33712.
- [154] X. Wang, L. Lv, Z. Cheng, J. Gao, L. Dong, C. Hu, L. Qu, *Adv. Energy Mater.* **2016**, *6*, 1502100.
- [155] J. Xu, Y. Lin, J. W. Connell, L. Dai, *Small* **2015**, *11*, 6179.
- [156] J. Sun, L. Wang, R. Song, S. Yang, *RSC Adv.* **2015**, *5*, 91114.
- [157] Y. Lin, X. Han, C. J. Campbell, J.-W. Kim, B. Zhao, W. Luo, J. Dai, L. Hu, J. W. Connell, *Adv. Funct. Mater.* **2015**, *25*, 2920.
- [158] S. Shanmugam, S. Nachimuthu, V. Subramaniam, *Materials Today Communications* **2020**, *22*, 100714.
- [159] M. J. Lee, K. Lee, J. Lim, M. Li, S. Noda, S. J. Kwon, B. DeMatta, B. Lee, S. W. Lee, *Adv. Funct. Mater.* **2021**, *31*, 2009397.
- [160] X. Fan, W. T. Zheng, J.-L. Kuo, *ACS Appl. Mater. Interfaces* **2012**, *4*, 2432.
- [161] D. Das, S. Kim, K.-R. Lee, A. K. Singh, *Phys. Chem. Chem. Phys.* **2013**, *15*, 15128.
- [162] H. Yildirim, A. Kinaci, Z.-J. Zhao, M. K. Y. Chan, J. P. Greeley, *ACS Appl. Mater. Interfaces* **2014**, *6*, 21141.
- [163] Y. Okamoto, *J. Phys. Chem. C* **2016**, *120*, 14009.
- [164] D. Sun, J. Yang, X. Yan, *Chem. Commun.* **2015**, *51*, 2134.
- [165] S. Yang, X. Feng, L. Zhi, Q. Cao, J. Maier, K. Müllen, *Adv. Mater.* **2010**, *22*, 838.
- [166] D. Cai, L. Ding, S. Wang, Z. Li, M. Zhu, H. Wang, *Electrochim. Acta* **2014**, *139*, 96.
- [167] P. Guo, H. Song, X. Chen, *J. Mater. Chem.* **2010**, *20*, 4867.
- [168] R.-R. Yao, D.-L. Zhao, L.-Z. Bai, N.-N. Yao, L. Xu, *Nanoscale Res. Lett.* **2014**, *9*, 368.
- [169] K.-H. Lin, C.-L. Kuo, *J. Mater. Chem. A* **2017**, *5*, 4912.
- [170] D. Damien, B. Babu, T. N. Narayanan, A. L. Reddy, P. M. Ajayan, M. M. Shajumon, *Graphene* **2013**, *1*, 37.
- [171] H. Kuzmany, L. Shi, M. Martinati, S. Cambré, W. Wenseleers, J. Kürti, J. Kolta, G. Kukucska, K. Cao, U. Kaiser, T. Saito, T. Pichler, *Carbon* **2021**, *171*, 221.
- [172] S. Dutta, S. K. Pati, *J. Mater. Chem.* **2010**, *20*, 8207.
- [173] X. H. Liu, J. W. Wang, Y. Liu, H. Zheng, A. Kushima, S. Huang, T. Zhu, S. X. Mao, J. Li, S. Zhang, W. Lu, J. M. Tour, J. Y. Huang, *Carbon* **2012**, *50*, 3836.
- [174] D. V. Kosynkin, W. Lu, A. Sinitskii, G. Pera, Z. Sun, J. M. Tour, *ACS Nano* **2011**, *5*, 968.
- [175] B. Xiao, X. Li, X. Li, B. Wang, C. Langford, R. Li, X. Sun, *J. Phys. Chem. C* **2014**, *118*, 881.
- [176] Y. Liu, X. Wang, W. Wan, L. Li, Y. Dong, Z. Zhao, J. Qiu, *Nanoscale* **2016**, *8*, 2159.
- [177] Y. Liu, X. Wang, Y. Dong, Z. Wang, Z. Zhao, J. Qiu, *J. Mater. Chem. A* **2014**, *2*, 16832.
- [178] N. Wei, L. Yu, Z. Sun, Y. Song, M. Wang, Z. Tian, Y. Xia, J. Cai, Y. Li, L. Zhao, Q. Li, M. H. Rümmeli, J. Sun, Z. Liu, *ACS Nano* **2019**, *13*, 7517.
- [179] A. R. Thiruppathi, B. Sidhureddy, M. Salverda, P. C. Wood, A. Chen, *Electroanal. Chem.* **2020**, *875*, 113911.
- [180] C. Ma, X. Shao, D. Cao, *J. Mater. Chem.* **2012**, *22*, 8911.
- [181] X. Kong, Q. Chen, *Phys. Chem. Chem. Phys.* **2013**, *15*, 12982.
- [182] D. H. Wu, Y. F. Li, Z. Zhou, *Theor. Chem. Acc.* **2011**, *130*, 209.
- [183] Y.-X. Yu, *Phys. Chem. Chem. Phys.* **2013**, *15*, 16819.
- [184] Z.-S. Wu, W. Ren, L. Xu, F. Li, H.-M. Cheng, *ACS Nano* **2011**, *5*, 5463.
- [185] J. D. Bagley, D. K. Kumar, K. A. See, N.-C. Yeh, *RSC Adv.* **2020**, *10*, 39562.
- [186] Md. M. Islam, C. M. Subramaniyam, T. Akhter, S. N. Faisal, A. I. Minett, H. K. Liu, K. Konstantinov, S. X. Dou, *J. Mater. Chem. A* **2017**, *5*, 5290.
- [187] W. Ai, J. Li, Z. Du, C. Zou, H. Du, X. Xu, Y. Chen, H. Zhang, J. Zhao, C. Li, W. Huang, T. Yu, *Nano Res.* **2018**, *11*, 4562.
- [188] X. Wang, Z. Zeng, H. Ahn, G. Wang, *Appl. Phys. Lett.* **2009**, *95*, 183103.
- [189] J. Wang, Y. Xia, Y. Liu, W. Li, D. Zhao, *Energy Storage Mater.* **2019**, *22*, 147.
- [190] N. Yang, X. Zheng, L. Li, J. Li, Z. Wei, *J. Phys. Chem. C* **2017**, *121*, 19321.
- [191] J. Chen, C. Wu, C. Tang, W. Zhao, M. Xu, C. M. Li, *ChemistrySelect* **2017**, *2*, 5518.
- [192] I. Obraztsov, A. Bakandritsos, V. Šedajová, R. Langer, P. Jakubec, G. Zoppellaro, M. Pykal, V. Presser, M. Otyepka, R. Zbořil, *Adv. Energy Mater.* **2022**, *12*, 2103010.
- [193] A. Bakandritsos, M. Pykal, P. Błoński, P. Jakubec, D. D. Chronopoulos, K. Poláková, V. Georgakilas, K. Čépe, O. Tomanec, V. Ranc, A. B. Bourlinos, R. Zbořil, M. Otyepka, *ACS Nano* **2017**, *11*, 2982.
- [194] H. R. Lee, Y.-S. Kim, Y.-K. Lee, S. Lee, H.-I. Joh, *Int. J. Energy Res.* **2022**, *46*, 2021.
- [195] N.-N. Chai, J. Zeng, K.-G. Zhou, Y.-L. Xie, H.-X. Wang, H.-L. Zhang, C. Xu, J.-X. Zhu, Q.-Y. Yan, *Chem. Eur. J.* **2013**, *19*, 5948.
- [196] J. Xu, I.-Y. Jeon, J.-M. Seo, S. Dou, L. Dai, J.-B. Baek, *Adv. Mater.* **2014**, *26*, 7317.
- [197] P. Arunkumar, A. G. Ashish, B. Babu, S. Sarang, A. Suresh, C. H. Sharma, M. Thalakulam, M. M. Shajumon, *RSC Adv.* **2015**, *5*, 59997.
- [198] A. G. Ashish, P. Arunkumar, B. Babu, P. Manikandan, S. Sarang, M. M. Shajumon, *Electrochim. Acta* **2015**, *176*, 285.
- [199] S. P. Varghese, B. Babu, R. Prasannachandran, R. Antony, M. M. Shajumon, *J. Alloys Compd.* **2019**, *780*, 588.
- [200] S. P. Varghese, B. Babu, V. Surendran, D. Damien, R. Antony, M. M. Shajumon, *J. Energy Storage* **2022**, *47*, 103636.
- [201] L. F. Cui, X. P. Wang, N. Chen, G. F. Zhang, L. T. Qu, *J. Mater. Chem. A* **2017**, *5*, 14508.
- [202] B. Liu, J.-G. Zhang, G. Shen, *Nano Today* **2016**, *11*, 82.
- [203] S. Lin, J. Tang, W. Zhang, K. Zhang, Y. Chen, R. Gao, H. Yin, X. Yu, L.-C. Qin, *RSC Adv.* **2022**, *12*, 12590.
- [204] M. F. El-Kady, V. Strong, S. Dubin, R. B. Kaner, *Science* **2012**, *335*, 1326.
- [205] G. Zhou, F. Li, H.-M. Cheng, *Energy Environ. Sci.* **2014**, *7*, 1307.
- [206] Y. Hu, X. Sun, *J. Mater. Chem. A* **2014**, *2*, 10712.
- [207] J. Bi, Z. Du, J. Sun, Y. Liu, K. Wang, H. Du, W. Ai, W. Huang, *Adv. Mater.* **2023**, *35*, 2210734.
- [208] T. Tao, S. Lu, Y. Chen, *Advanced Materials Technologies* **2018**, *3*, 1700375.
- [209] C. Dai, G. Sun, L. Hu, Y. Xiao, Z. Zhang, L. Qu, *InfoMat.* **2020**, *2*, 509.
- [210] S. Iijima, *Nature* **1991**, *354*, 56.
- [211] P. M. Ajayan, *Chem. Rev.* **1999**, *99*, 1787.
- [212] Y. Ando, X. Zhao, H. Shimoyama, G. Sakai, K. Kaneto, *Int. J. Inorg. Mater.* **1999**, *1*, 77.
- [213] G. Van Lier, C. Van Alsenoy, V. Van Doren, P. Geerlings, *Chem. Phys. Lett.* **2000**, *326*, 181.
- [214] N. Anzar, R. Hasan, M. Tyagi, N. Yadav, J. Narang, *Sensors International* **2020**, *1*, 100003.
- [215] D. Tasis, N. Tagmatarchis, A. Bianco, M. Prato, *Chem. Rev.* **2006**, *106*, 1105.
- [216] M. M. J. Treacy, T. W. Ebbesen, J. M. Gibson, *Nature* **1996**, *381*, 678.
- [217] B. J. Landi, M. J. Ganter, C. D. Cress, R. A. DiLeo, R. P. Raffaelle, *Energy Environ. Sci.* **2009**, *2*, 638.
- [218] C. de las Casas, W. Li, *J. Power Sources* **2012**, *208*, 74.
- [219] P. Sehrawat, C. Julien, S. S. Islam, *Mater. Sci. Eng. B* **2016**, *213*, 12.
- [220] D. Di Lecce, P. Andreotti, M. Boni, G. Gasparro, G. Rizzati, J.-Y. Hwang, Y.-K. Sun, J. Hassoun, *ACS Sustainable Chem. Eng.* **2018**, *6*, 3225.
- [221] Z. Xiong, Y. S. Yun, H.-J. Jin, *Materials* **2013**, *6*, 1138.
- [222] X.-M. Liu, Z. dong Huang, S. woon Oh, B. Zhang, P.-C. Ma, M. M. F. Yuen, J.-K. Kim, *Compos. Sci. Technol.* **2012**, *72*, 121.
- [223] Z. Fang, J. Wang, H. Wu, Q. Li, S. Fan, J. Wang, *J. Power Sources* **2020**, *454*, 227932.
- [224] S. Y. Chew, S. H. Ng, J. Wang, P. Novák, F. Krumeich, S. L. Chou, J. Chen, H. K. Liu, *Carbon* **2009**, *47*, 2976.
- [225] H. Shimoda, B. Gao, X. P. Tang, A. Kleinhammes, L. Fleming, Y. Wu, O. Zhou, *Phys. Rev. Lett.* **2001**, *88*, 015502.
- [226] J. Zhao, A. Buldum, J. Han, J. Ping Lu, *Phys. Rev. Lett.* **2000**, *85*, 1706.
- [227] S. Yang, H. Song, X. Chen, A. V. Okotrub, L. G. Bulusheva, *Electrochim. Acta* **2007**, *52*, 5286.
- [228] S. Yang, J. Huo, H. Song, X. Chen, *Electrochim. Acta* **2008**, *53*, 2238.
- [229] Y. Liu, H. Yukawa, M. Morinaga, *Comput. Mater. Sci.* **2004**, *30*, 50.
- [230] T. Kar, J. Pattayanayak, S. Scheiner, *J. Phys. Chem. A* **2001**, *105*, 10397.
- [231] C. Garau, A. Frontera, D. Quiñonero, A. Costa, P. Ballester, P. M. Deyà, *Chem. Phys. Lett.* **2003**, *374*, 548.
- [232] V. Meunier, J. Kephart, C. Roland, J. Bernholc, *Phys. Rev. Lett.* **2AD**, *88*, 075506.
- [233] K. Nishidate, M. Hasegawa, *Phys. Rev. B* **6AD**, *71*, 245418.
- [234] S. A. Sozykin, V. P. Beskachko, *Diamond Relat. Mater.* **2017**, *79*, 127.
- [235] A. Udomvech, T. Kerdcharoen, T. Osotchan, *Chem. Phys. Lett.* **2005**, *406*, 161.
- [236] S. Kawasaki, T. Hara, Y. Iwai, Y. Suzuki, *Mater. Lett.* **2008**, *62*, 2917.
- [237] X. X. Wang, J. N. Wang, H. Chang, Y. F. Zhang, *Adv. Funct. Mater.* **2007**, *17*, 3613.
- [238] C. Masarapu, V. Subramanian, H. Zhu, B. Wei, *Adv. Funct. Mater.* **2009**, *19*, 1008.
- [239] J. Y. Eom, H. S. Kwon, J. Liu, O. Zhou, *Carbon* **2004**, *42*, 2589.
- [240] J. Eom, D. Kim, H. Kwon, *J. Power Sources* **2006**, *157*, 507.
- [241] Z. Yang, H.-Q. Wu, B. Simard, *Electrochim. Commun.* **2002**, *4*, 574.
- [242] S. W. Lee, N. Yabuuchi, B. M. Gallant, S. Chen, B.-S. Kim, P. T. Hammond, Y. Shao-Horn, *Nat. Nanotechnol.* **2010**, *5*, 531.

- [243] I. Zeferino González, H.-C. Chiu, R. Gauvin, G. P. Demopoulos, Y. Verde-Gómez, *Materials Today Communications* **2022**, *30*, 103158.
- [244] X. Li, J. Liu, Y. Zhang, Y. Li, H. Liu, X. Meng, J. Yang, D. Geng, D. Wang, R. Li, X. Sun, *J. Power Sources* **2012**, *197*, 238.
- [245] W. H. Shin, H. M. Jeong, B. G. Kim, J. K. Kang, J. W. Choi, *Nano Lett.* **2012**, *12*, 2283.
- [246] H. Byeon, B. Gu, H.-J. Kim, J. H. Lee, I. Seo, J. Kim, J. W. Yang, J.-K. Kim, *Chem. Eng. J.* **2021**, *413*, 127402.
- [247] B. Liu, X. Sun, Z. Liao, X. Lu, L. Zhang, G.-P. Hao, *Sci. Rep.* **2021**, *11*, 5633.
- [248] W. J. Lee, J. Lim, S. O. Kim, *Small Methods* **2017**, *1*, 1600014.
- [249] S. H. Lim, R. Li, W. Ji, J. Lin, *Phys. Rev. B* **11AD**, *76*, 195406.
- [250] L. G. Bulusheva, A. V. Okotrub, A. G. Kurenya, H. Zhang, H. Zhang, X. Chen, H. Song, *Carbon* **2011**, *49*, 4013.
- [251] C.-C. Kaun, B. Larade, H. Mehrez, J. Taylor, H. Guo, *Phys. Rev. B* **5AD**, *65*, 205416.
- [252] B. Zhang, Y. Yu, Z.-L. Xu, S. Abouali, M. Akbari, Y.-B. He, F. Kang, J.-K. Kim, *Adv. Energy Mater.* **2014**, *4*, 1301448.
- [253] T. Maitra, S. Sharma, A. Srivastava, Y.-K. Cho, M. Madou, A. Sharma, *Carbon* **2012**, *50*, 1753.
- [254] S. Chen, L. Qiu, H.-M. Cheng, *Chem. Rev.* **2020**, *120*, 2811.
- [255] D. Ma, X. Mu, G. Zhao, X. Qin, M. Qi, *Coating* **2023**, *13*.
- [256] W. Li, M. Li, K. R. Adair, X. Sun, Y. Yu, *J. Mater. Chem. A* **2017**, *5*, 13882.
- [257] B.-S. Lee, S.-B. Son, K.-M. Park, W.-R. Yu, K.-H. Oh, S.-H. Lee, *J. Power Sources* **2012**, *199*, 53.
- [258] L. Ji, Y. Yao, O. Toprakci, Z. Lin, Y. Liang, Q. Shi, A. J. Medford, C. R. Millns, X. Zhang, *J. Power Sources* **2010**, *195*, 2050.
- [259] G. Wang, M. Yu, X. Feng, *Chem. Soc. Rev.* **2021**, *50*, 2388.
- [260] N. M. Rodriguez, *J. Mater. Res.* **2011**, *8*, 3233.
- [261] R. Zheng, Y. Zhao, H. Liu, C. Liang, G. Cheng, *Carbon* **2006**, *44*, 742.
- [262] Z.-Y. Wu, C. Li, H.-W. Liang, J.-F. Chen, S.-H. Yu, *Angew. Chem. Int. Ed.* **2013**, *52*, 2925.
- [263] W. Wang, Y. Sun, B. Liu, S. Wang, M. Cao, *Carbon* **2015**, *91*, 56.
- [264] C. Kim, K. S. Yang, M. Kojima, K. Yoshida, Y. J. Kim, Y. A. Kim, M. Endo, *Adv. Funct. Mater.* **2006**, *16*, 2393.
- [265] X. Yang, Y. Chen, C. Zhang, G. Duan, S. Jiang, *Composites Part B* **2023**, *249*, 110386.
- [266] M. Inagaki, Y. Yang, F. Kang, *Adv. Mater.* **2012**, *24*, 2547.
- [267] T. D. Nguyen, J. S. Lee, *Applied Sciences* **2022**, *12*.
- [268] G. Wang, C. Pan, L. Wang, Q. Dong, C. Yu, Z. Zhao, J. Qiu, *Electrochim. Acta* **2012**, *69*, 65.
- [269] B. Zhang, F. Kang, J.-M. Tarascon, J.-K. Kim, *Prog. Mater. Sci.* **2016**, *76*, 319.
- [270] B. Joshi, E. Samuel, Y. Kim, A. L. Yarin, M. T. Swihart, S. S. Yoon, *Chem. Eng. J.* **2022**, *430*, 132876.
- [271] Y. Zhao, J. Yan, J. Yu, B. Ding, *Macromol. Rapid Commun.* **2023**, *44*, 2200740.
- [272] X. Hu, G. Zhong, J. Li, Y. Liu, J. Yuan, J. Chen, H. Zhan, Z. Wen, *Energy Environ. Sci.* **2020**, *13*, 2431.
- [273] L. Ji, X. Zhang, *Nanotechnology* **2009**, *20*, 155705.
- [274] L. Qie, W.-M. Chen, Z.-H. Wang, Q.-G. Shao, X. Li, L.-X. Yuan, X.-L. Hu, W.-X. Zhang, Y.-H. Huang, *Adv. Mater.* **2012**, *24*, 2047.
- [275] Y. Xing, Y. Wang, C. Zhou, S. Zhang, B. Fang, *ACS Appl. Mater. Interfaces* **2014**, *6*, 2561.
- [276] W. Li, M. Li, M. Wang, L. Zeng, Y. Yu, *Nano Energy* **2015**, *13*, 693.
- [277] Z. Wang, X. Xiong, L. Qie, Y. Huang, *Electrochim. Acta* **2013**, *106*, 320.
- [278] D. Nan, Z.-H. Huang, R. Lv, L. Yang, J.-G. Wang, W. Shen, Y. Lin, X. Yu, L. Ye, H. Sun, F. Kang, *J. Mater. Chem. A* **2014**, *2*, 19678.
- [279] Y. Chen, X. Li, X. Zhou, H. Yao, H. Huang, Y.-W. Mai, L. Zhou, *Energy Environ. Sci.* **2014**, *7*, 2689.
- [280] H. Zhao, H. Yin, X.-X. Yu, W. Zhang, C. Li, M.-Q. Zhu, *J. Alloys Compd.* **2018**, *735*, 319.
- [281] K. Yan, S. Chen, J. Zhai, Y. Zhao, Z. Deng, G. Wang, *Energy Technol.* **2020**, *8*, 2000219.
- [282] G.-H. An, D.-Y. Lee, H.-J. Ahn, *ACS Appl. Mater. Interfaces* **2017**, *9*, 12478.
- [283] Yunhua Yu, Yuan Liu, Xiaoping Yang, In *Alkali-ion Batteries* (Ed.: Dongfang Yang), IntechOpen, Rijeka, **2016**, p. Ch. 1.
- [284] S. Praveen, G. S. Sim, C. W. Ho, C. W. Lee, *Energy Storage Mater.* **2021**, *41*, 748.
- [285] X. Zhang, Q. Huang, M. Zhang, M. Li, J. Hu, G. Yuan, *J. Alloys Compd.* **2020**, *822*, 153718.
- [286] H. Lu, J. Hagberg, G. Lindbergh, A. Cornell, *Batteries* **2018**, *4*.
- [287] F. Zhao, X. Zhao, B. Peng, F. Gan, M. Yao, W. Tan, J. Dong, Q. Zhang, *Chin. Chem. Lett.* **2018**, *29*, 1692.
- [288] A. Yadav, B. De, S. K. Singh, P. Sinha, K. K. Kar, *ACS Appl. Mater. Interfaces* **2019**, *11*, 7974.
- [289] C. Sun, Z. Han, X. Wang, B. Liu, Q. Li, H. Li, J. Xu, J.-M. Cao, X.-L. Wu, *Adv. Funct. Mater.* **2023**, *n/a*, 2305606.
- [290] B. Guo, X. Yu, X.-G. Sun, M. Chi, Z.-A. Qiao, J. Liu, Y.-S. Hu, X.-Q. Yang, J. B. Goodenough, S. Dai, *Energy Environ. Sci.* **2014**, *7*, 2220.
- [291] F. Wang, R. Robert, N. A. Chernova, N. Pereira, F. Omeyna, F. Badway, X. Hua, M. Ruotolo, R. Zhang, L. Wu, V. Volkov, D. Su, B. Key, M. S. Whittingham, C. P. Grey, G. G. Amatucci, Y. Zhu, J. Graetz, *J. Am. Chem. Soc.* **2011**, *133*, 18828.
- [292] S.-H. Yu, X. Feng, N. Zhang, J. Seok, H. D. Abruna, *Acc. Chem. Res.* **2018**, *51*, 273.
- [293] H. S. Ryu, H. J. Ahn, K. W. Kim, J. H. Ahn, K. K. Cho, T. H. Nam, *Electrochim. Acta* **2006**, *52*, 1563.
- [294] J. Cabana, L. Monconduit, D. Larcher, M. R. Palacín, *Adv. Mater.* **2010**, *22*, E170.
- [295] M. N. Obrovac, V. L. Chevrier, *Chem. Rev.* **2014**, *114*, 11444.
- [296] J. Li, S. Hwang, F. Guo, S. Li, Z. Chen, R. Kou, K. Sun, C.-J. Sun, H. Gan, A. Yu, E. A. Stach, H. Zhou, D. Su, *Nat. Commun.* **2019**, *10*, 2224.
- [297] F. Dou, L. Shi, G. Chen, D. Zhang, *Electrochemical Energy Reviews* **2019**, *2*, 149.
- [298] F. Luo, B. Liu, J. Zheng, G. Chu, K. Zhong, H. Li, X. Huang, L. Chen, *J. Electrochem. Soc.* **2015**, *162*, A2509.
- [299] H. Wang, L.-F. Cui, Y. Yang, H. Sanchez Casalongue, J. T. Robinson, Y. Liang, Y. Cui, H. Dai, *J. Am. Chem. Soc.* **2010**, *132*, 13978.
- [300] W.-R. Liu, Y.-C. Yen, H.-C. Wu, M. Winter, N.-L. Wu, *J. Appl. Electrochem.* **2009**, *39*, 1643.
- [301] X. Shen, Z. Tian, R. Fan, L. Shao, D. Zhang, G. Cao, L. Kou, Y. Bai, *J. Energy Chem.* **2018**, *27*, 1067.
- [302] Y. R. Jhan, J. G. Duh, *J. Power Sources* **2012**, *198*, 294.
- [303] Z. Cao, Y. Yang, J. Qin, Z. Su, *J. Power Sources* **2021**, *491*, 229577.
- [304] H. Zeng, B. Xing, C. Zhang, L. Chen, H. Zhao, X. Han, G. Yi, G. Huang, C. Zhang, Y. Cao, *Energy Fuels* **2020**, *34*, 2480.
- [305] Y.-S. Hsiao, L.-Y. Chang, C.-W. Hu, C.-Z. Lu, N.-J. Wu, Y.-L. Chen, T.-H. Hsieh, J.-H. Huang, S.-C. Hsu, H.-C. Weng, C.-P. Chen, *Appl. Surf. Sci.* **2023**, *614*, 156155.
- [306] S. Li, C. Pan, Z. Zhao, W. Yang, H. Zou, S. Chen, *Dalton Trans.* **2023**.
- [307] Y. Ma, H. Qu, W. Wang, Y. Yu, X. Zhang, B. Li, L. Wang, *Adv. Funct. Mater.* **2023**, *33*, 2211648.
- [308] J. Lee, G. Oh, H.-Y. Jung, J.-Y. Hwang, *Inorganics* **2023**, *11*.
- [309] L. Sun, Y. Liu, R. Shao, J. Wu, R. Jiang, Z. Jin, *Energy Storage Mater.* **2022**, *46*, 482.
- [310] Y. Zhang, B. Wu, G. Mu, C. Ma, D. Mu, F. Wu, *J. Energy Chem.* **2022**, *64*, 615.
- [311] K. Feng, M. Li, W. Liu, A. G. Kashkooli, X. Xiao, M. Cai, Z. Chen, *Small* **2018**, *14*, 1702737.
- [312] X. Zhao, V.-P. Lehto, *Nanotechnology* **2020**, *32*, 042002.
- [313] C. K. Chan, H. Peng, G. Liu, K. McIlwrath, X. F. Zhang, R. A. Huggins, Y. Cui, *Nat. Nanotechnol.* **2008**, *3*, 31.
- [314] Y. He, L. Jiang, T. Chen, Y. Xu, H. Jia, R. Yi, D. Xue, M. Song, A. Genc, C. Bouchet-Marquis, L. Pullan, T. Tessner, J. Yoo, X. Li, J.-G. Zhang, S. Zhang, C. Wang, *Nat. Nanotechnol.* **2021**, *16*, 1113.
- [315] Z. Chen, A. Soltani, Y. Chen, Q. Zhang, A. Davoodi, S. Hosseinpour, W. Peukert, W. Liu, *Adv. Energy Mater.* **2022**, *12*, 2200924.
- [316] X. Zhang, D. Wang, X. Qiu, Y. Ma, D. Kong, K. Müllen, X. Li, L. Zhi, *Nat. Commun.* **2020**, *11*, 3826.
- [317] I. Zilberman, J. Sturm, A. Jossen, *J. Power Sources* **2019**, *425*, 217.
- [318] B. Wang, X. Li, X. Zhang, B. Luo, M. Jin, M. Liang, S. A. Dayeh, S. T. Picraux, L. Zhi, *ACS Nano* **2013**, *7*, 1437.
- [319] X. Zhou, Y.-X. Yin, L.-J. Wan, Y.-G. Guo, *Chem. Commun.* **2012**, *48*, 2198.
- [320] Y. Bai, X. Cao, Z. Tian, S. Yang, G. Cao, *Nano Express* **2021**, *2*, 010021.
- [321] X. Li, P. Yan, X. Xiao, J. H. Woo, C. Wang, J. Liu, J.-G. Zhang, *Energy Environ. Sci.* **2017**, *10*, 1427.
- [322] X. Li, D. Yang, X. Hou, J. Shi, Y. Peng, H. Yang, *J. Alloys Compd.* **2017**, *728*, 1.
- [323] J. Li, J. Wang, J. Yang, X. Ma, S. Lu, *J. Alloys Compd.* **2016**, *688*, 1072.
- [324] P. Li, J.-Y. Hwang, Y.-K. Sun, *ACS Nano* **2019**, *13*, 2624.
- [325] R. Cong, J.-Y. Choi, J.-B. Song, M. Jo, H. Lee, C.-S. Lee, *Sci. Rep.* **2021**, *11*, 1283.
- [326] J.-G. Ren, C. Wang, Q.-H. Wu, X. Liu, Y. Yang, L. He, W. Zhang, *Nanoscale* **2014**, *6*, 3353.
- [327] S. K. Kim, H. Kim, H. Chang, B.-G. Cho, J. Huang, H. Yoo, H. Kim, H. D. Jang, *Sci. Rep.* **2016**, *6*, 33688.
- [328] M. Tokur, M. Y. Jin, B. W. Sheldon, H. Akbulut, *ACS Appl. Mater. Interfaces* **2020**, *12*, 33855.

- [329] Y. Huang, W. Li, J. Peng, Z. Wu, X. Li, X. Wang, *Energy Fuels* **2021**, *35*, 13491.
- [330] J. Zhou, Y. Lan, K. Zhang, G. Xia, J. Du, Y. Zhu, Y. Qian, *Nanoscale* **2016**, *8*, 4903.
- [331] L. K. Ventrapragada, P. Parajuli, A. B. Kousalya, S. Pilla, R. Podila, A. M. Rao, *ECS Meeting Abstracts* **2017**, MA2017-01, 489.
- [332] M. Hamza, S. Zhang, W. Xu, D. Wang, Y. Ma, X. Li, *Nanoscale* **2023**, *15*, 14338.
- [333] Y. Pei, Y. Wang, A.-Y. Chang, Y. Liao, S. Zhang, X. Wen, S. Wang, *Carbon* **2023**, *203*, 436.
- [334] K. Fu, Y. Lu, M. Dirican, C. Chen, M. Yanilmaz, Q. Shi, P. D. Bradford, X. Zhang, *Nanoscale* **2014**, *6*, 7489.
- [335] J. Hong, J. Zhang, X. Li, Y. Guo, X. Zhou, Z. Liu, *ACS Appl. Nano Mater.* **2023**, *6*, 10138.
- [336] K. Fu, O. Yildiz, H. Bhanushali, Y. Wang, K. Stano, L. Xue, X. Zhang, P. D. Bradford, *Adv. Mater.* **2013**, *25*, 5109.
- [337] T. H. Hwang, Y. M. Lee, B.-S. Kong, J.-S. Seo, J. W. Choi, *Nano Lett.* **2012**, *12*, 802.
- [338] Z. Yu, L. Cui, B. Zhong, G. Qu, *Coating* **2023**, *13*.
- [339] A. Du, H. Li, X. Chen, Y. Han, Z. Zhu, C. Chu, *ChemistrySelect* **2022**, *7*, e202201269.
- [340] T. Najam, M. K. Aslam, K. Rafiq, M. Altaf Nazir, A. ur Rehman, M. Imran, M. S. Javed, X. Cai, S. S. A. Shah, *Mater. Sci. Eng. B* **2021**, *273*, 115417.
- [341] H. Ye, G. Zheng, X. Yang, D. Zhang, Y. Zhang, S. Yan, L. You, S. Hou, Z. Huang, *J. Electroanal. Chem.* **2021**, *898*, 115652.
- [342] P. Divya, N. G. Prakash, T. J. Ko, P. Rosaiah, *J. Cluster Sci.* **2023**, *34*, 2103.
- [343] L. Wu, Y. Liu, H. Zhao, Z. Wang, B. Zhu, X. Zhang, P. He, Y. Liu, T. Yang, *ACS Omega* **2022**, *7*, 16837.
- [344] B. Lung-Hao Hu, F.-Y. Wu, C.-T. Lin, A. N. Khlobystov, L.-J. Li, *Nat. Commun.* **2013**, *4*, 1687.
- [345] C. W. Park, J.-H. Lee, J. K. Seo, W. Y. Jo, D. Whang, S. M. Hwang, Y.-J. Kim, *Nat. Commun.* **2021**, *12*, 2145.
- [346] H. Wu, Q. Liu, S. Guo, *Nano-Micro Lett.* **2014**, *6*, 316.
- [347] M. Sathiya, A. S. Prakash, K. Ramesha, J. Tarascon, A. K. Shukla, *J. Am. Chem. Soc.* **2011**, *133*, 16291.
- [348] Z.-S. Wu, W. Ren, L. Wen, L. Gao, J. Zhao, Z. Chen, G. Zhou, F. Li, H.-M. Cheng, *ACS Nano* **2010**, *4*, 3187.
- [349] B. Lu, B. Ma, X. Deng, B. Wu, Z. Wu, J. Luo, X. Wang, G. Chen, *Chem. Eng. J.* **2018**, *351*, 269.
- [350] W. Wang, P. N. Kumta, *ACS Nano* **2010**, *4*, 2233.
- [351] L.-F. Cui, L. Hu, J. W. Choi, Y. Cui, *ACS Nano* **2010**, *4*, 3671.
- [352] M. Wu, C. Wang, J. Chen, F. Wang, B. Yi, *Ionics* **2013**, *19*, 1341.
- [353] M. Liu, S. Zhang, H. Dong, X. Chen, S. Gao, Y. Sun, W. Li, J. Xu, L. Chen, A. Yuan, W. Lu, *ACS Sustainable Chem. Eng.* **2019**, *7*, 4195.
- [354] Z. Fang, W. Xu, T. Huang, M. Li, W. Wang, Y. Liu, C. Mao, F. Meng, M. Wang, M. Cheng, A. Yu, X. Guo, *Mater. Res. Bull.* **2013**, *48*, 4419.
- [355] S.-H. Park, W.-J. Lee, *J. Power Sources* **2015**, *281*, 301.
- [356] S. Gao, N. Wang, S. Li, D. Li, Z. Cui, G. Yue, J. Liu, X. Zhao, L. Jiang, Y. Zhao, *Angew. Chem. Int. Ed.* **2020**, *59*, 2465.
- [357] M.-L. Chen, Q. Zhang, J. Wang, X.-X. Zhu, C.-F. Zhao, F.-H. Cao, H. Li, C.-L. Zhang, *ACS Appl. Energ. Mater.* **2023**, *6*, 4942.
- [358] L. Chen, B. Tang, H. Li, B. Wang, B. Huang, *Solid State Ionics* **2023**, *396*, 116241.
- [359] C. Gao, Z. Jiang, P. Wang, L. R. Jensen, Y. Zhang, Y. Yue, *Nano Energy* **2020**, *74*, 104868.
- [360] S. H. Choi, J.-H. Lee, Y. C. Kang, *ACS Nano* **2015**, *9*, 10173.
- [361] J. Li, F. Dou, J. Gong, Y. Gao, Y. Hua, K. Sielicki, D. Zhang, E. Mijowska, X. Chen, *ACS Appl. Nano Mater.* **2023**, *6*, 1171.
- [362] C. Zhu, Y. Zhang, Y. Ye, G. Li, F. Cheng, *ACS Appl. Mater. Interfaces* **2023**, *15*, 39363.
- [363] B. Cao, Z. Liu, C. Xu, J. Huang, H. Fang, Y. Chen, *J. Power Sources* **2019**, *414*, 233.
- [364] X. Ou, L. Cao, X. Liang, F. Zheng, H.-S. Zheng, X. Yang, J.-H. Wang, C. Yang, M. Liu, *ACS Nano* **2019**, *13*, 3666.
- [365] J. Huang, Y. Ma, Q. Xie, H. Zheng, J. Yang, L. Wang, D.-L. Peng, *Small* **2018**, *14*, 1703513.
- [366] Y. Sun, H.-W. Lee, Z. W. Seh, N. Liu, J. Sun, Y. Li, Y. Cui, *Nat. Energy* **2016**, *1*, 15008.
- [367] J. P. Zheng, P. Andrei, L. Jin, J. Zheng, C. Zhang, *J. Electrochem. Soc.* **2022**, *169*, 040532.
- [368] S. Park, S. Y. Jeong, T. K. Lee, M. W. Park, H. Y. Lim, J. Sung, J. Cho, S. K. Kwak, S. Y. Hong, N.-S. Choi, *Nat. Commun.* **2021**, *12*, 838.
- [369] K. Kim, H. Ma, S. Park, N.-S. Choi, *ACS Energy Lett.* **2020**, *5*, 1537.
- [370] J. Ming, Z. Cao, Y. Wu, W. Wahyudi, W. Wang, X. Guo, L. Cavallo, J.-Y. Hwang, A. Shamim, L.-J. Li, Y.-K. Sun, H. N. Alshareef, *ACS Energy Lett.* **2019**, *4*, 2613.
- [371] Y. Sun, Y. Li, J. Sun, Y. Li, A. Pei, Y. Cui, *Energy Storage Mater.* **2017**, *6*, 119.
- [372] Z. Li, H. Rao, R. Atwi, B. M. Sivakumar, B. Gwalani, S. Gray, K. S. Han, T. A. Everett, T. A. Ajantiwalay, V. Murugesan, N. N. Rajput, V. G. Pol, *Nat. Commun.* **2023**, *14*, 868.
- [373] X. Wang, M. Salari, D. Jiang, J. Chapman Varela, B. Anasori, D. J. Wesolowski, S. Dai, M. W. Grinstaff, Y. Gogotsi, *Nat. Rev. Mater.* **2020**, *5*, 787.
- [374] Q. Li, J. Chen, L. Fan, X. Kong, Y. Lu, *Green Energy & Environment* **2016**, *1*, 18.
- [375] X. Ma, J. Yu, Y. Hu, J. Texter, F. Yan, *Ind. Chem. Mater.* **2023**, *1*, 39.

Manuscript received: November 16, 2023

Revised manuscript received: January 22, 2024

Accepted manuscript online: January 26, 2024

Version of record online: February 13, 2024